University of Kentucky
UKnowledge

Theses and Dissertations--Biomedical Engineering

Biomedical Engineering

2012

USE OF HYBRID DIFFUSE OPTICAL SPECTROSCOPIES IN CONTINUOUS MONITORING OF BLOOD FLOW, BLOOD OXYGENATION, AND OXYGEN CONSUMPTION RATE IN EXERCISING SKELETAL MUSCLE

Katelyn Gurley
University of Kentucky, kmgurl2@gmail.com

Recommended Citation
Gurley, Katelyn, "USE OF HYBRID DIFFUSE OPTICAL SPECTROSCOPIES IN CONTINUOUS MONITORING OF BLOOD FLOW, BLOOD OXYGENATION, AND OXYGEN CONSUMPTION RATE IN EXERCISING SKELETAL MUSCLE" (2012). *Theses and Dissertations--Biomedical Engineering*. 3.
http://uknowledge.uky.edu/cbme_etds/3

This Master's Thesis is brought to you for free and open access by the Biomedical Engineering at UKnowledge. It has been accepted for inclusion in Theses and Dissertations--Biomedical Engineering by an authorized administrator of UKnowledge. For more information, please contact UKnowledge@lsv.uky.edu.

STUDENT AGREEMENT:

I represent that my thesis or dissertation and abstract are my original work. Proper attribution has been given to all outside sources. I understand that I am solely responsible for obtaining any needed copyright permissions. I have obtained and attached hereto needed written permission statements(s) from the owner(s) of each third-party copyrighted matter to be included in my work, allowing electronic distribution (if such use is not permitted by the fair use doctrine).

I hereby grant to The University of Kentucky and its agents the non-exclusive license to archive and make accessible my work in whole or in part in all forms of media, now or hereafter known. I agree that the document mentioned above may be made available immediately for worldwide access unless a preapproved embargo applies.

I retain all other ownership rights to the copyright of my work. I also retain the right to use in future works (such as articles or books) all or part of my work. I understand that I am free to register the copyright to my work.

REVIEW, APPROVAL AND ACCEPTANCE

The document mentioned above has been reviewed and accepted by the student's advisor, on behalf of the advisory committee, and by the Director of Graduate Studies (DGS), on behalf of the program; we verify that this is the final, approved version of the student's dissertation including all changes required by the advisory committee. The undersigned agree to abide by the statements above.

Katelyn Gurley, Student

Dr. Guoqiang Yu, Major Professor

Dr. Abhijit Patwardhan, Director of Graduate Studies

USE OF HYBRID DIFFUSE OPTICAL SPECTROSCOPIES IN CONTINUOUS MONITORING OF BLOOD FLOW, BLOOD OXYGENATION, AND OXYGEN CONSUMPTION RATE IN EXERCISING SKELETAL MUSCLE

THESIS

A thesis submitted in partial fulfillment of the
requirements for the degree of Master of Science in Biomedical
Engineering in the Graduate School at the University of Kentucky

By

Katelyn Gurley

Lexington, Kentucky

Director: Dr. Guoqiang Yu, Associate Professor of Biomedical Engineering

Lexington, Kentucky

2012

Copyright © Katelyn Gurley 2012

ABSTRACT OF THESIS

USE OF HYBRID DIFFUSE OPTICAL SPECTROSCOPIES IN CONTINUOUS MONITORING OF BLOOD FLOW, BLOOD OXYGENATION, AND OXYGEN CONSUMPTION RATE IN EXERCISING SKELETAL MUSCLE

This study combines noninvasive hybrid diffuse optical spectroscopies [near-infrared spectroscopy (NIRS) and diffuse correlation spectroscopy (DCS)] with occlusive calibration for continuous measurement of absolute blood flow (BF), tissue blood oxygenation (S_tO_2), and oxygen consumption rate ($\dot{V}O_2$) in exercising skeletal muscle. Subjects performed rhythmic dynamic handgrip exercise, while an optical probe connected to a hybrid NIRS/DCS flow-oximeter directly monitored oxy-, deoxy-, and total hemoglobin concentrations ([HbO_2], [Hb], and [tHb]), S_tO_2, relative BF (rBF), and relative $\dot{V}O_2$ ($r\dot{V}O_2$) in the forearm flexor muscles. Absolute baseline BF and $\dot{V}O_2$ were obtained through venous and arterial occlusions, respectively, and used to calibrate continuous relative parameters. Previously known problems with muscle fiber motion artifact in optical measurements were mitigated with a novel dynamometer-based gating algorithm. Nine healthy young subjects were measured and results validated against previous literature findings. Ten older subjects with fibromyalgia and thirteen age-matched healthy controls were then successfully measured to observe differences in hemodynamic and metabolic response to exercise. This study demonstrates a novel application of NIRS/DCS technology to simultaneously evaluate quantitative hemodynamic and metabolic parameters in exercising skeletal muscle. This method has broad application to research and clinical assessment of disease (e.g. peripheral vascular disease, fibromyalgia), treatment evaluation, and sports medicine.

KEYWORDS: Diffuse correlation spectroscopy; near-infrared spectroscopy; blood flow; blood oxygenation; oxygen consumption rate

Katelyn Gurley

7/30/2012

USE OF HYBRID DIFFUSE OPTICAL SPECTROSCOPIES IN CONTINUOUS MONITORING OF BLOOD FLOW, BLOOD OXYGENATION, AND OXYGEN CONSUMPTION RATE IN EXERCISING SKELETAL MUSCLE

By

Katelyn Gurley

Dr. Guoqiang Yu
Director of Thesis

Dr. Abhijit Patwardhan
Director of Graduate Studies

7/30/2012

ACKNOWLEDGEMENTS

I would like to first thank my adviser, Dr. Guoqiang Yu, without whom this work would never have been possible. I greatly appreciate the opportunities he has provided, his technical advice and discussions regarding this work, and the inexhaustible enthusiasm he shows for technological development and scientific research.

I would also like to sincerely thank Dr. Yu Shang, who worked closely with me on this project, patiently assisting, despite his own full workload. I would like to thank Ran Cheng, for his assistance in all things technological and instrument-related, and for his positive attitude. I acknowledge all my lab-mates, both old and new. I appreciate their ideas and contributions, new perspectives, kind words, willingness to help, and for their general discipline and dedication. I am continually motivated by their achievements, and am very thankful to have had their company during my time in this lab.

I would like to thank everybody I have worked with in the College of Engineering, my home for the past 7 years. I would not be the person I am today without this place and the numerous talented individuals who work there. I would like to thank all of my collaborators, especially Dr. Leslie Crofford and Dr. Charlotte Peterson, for their intellect and insight. I am truly fortunate to work with such exceptional groups.

I would particularly like to thank my family, especially my parents and brothers, for being as equally diverse and interesting as they are brilliant and accomplished. In difficult times, they have given me great comfort, inspiration, and motivation.

Finally, I thank my friends, for balancing long days in the lab with long nights on the weekends. They continually provide me with personal insight and perspective, and I absolutely would not survive without them.

TABLE OF CONTENTS

LIST OF TABLES

LIST OF FIGURES

CHAPTER 1: INTRODUCTION

1.1 Blood Flow and Metabolism in Health and Disease

To produce energy for normal cellular function, living cells consume oxygen and produce metabolic waste via aerobic respiration. Nutrients are supplied and waste is removed via diffusion through capillary membranes in the microvasculature of the cardiovascular system, which is regulated by many factors, both centrally (central nervous system) and locally (mechano-chemical response). The balance of oxygen delivery and oxygen consumption is critical in maintaining homeostasis for health. In order to fully understand how certain tissues function, and the regulatory mechanisms that maintain their homeostatic environment, it is essential to monitor both the nutrient supply and consumption at a local level. As such, blood flow (BF), oxygen consumption rate ($\dot{V}O_2$), and tissue blood oxygen saturation (S_tO_2) can all provide useful metrics for evaluating tissue health and disease.

Skeletal muscle provides an excellent platform for studying cardiovascular and metabolic regulation, as it comprises approximately 40% of total body mass, and under working conditions, can utilize up to 85% of total cardiac output [1]. Characterization of circulatory and metabolic function in skeletal muscle has provided key insight into the pathophysiology, diagnosis, and treatment of common and widespread diseases affecting millions of people annually (e.g., 12–14 % of older adults in U.S. with peripheral arterial disease [2-4], 10 million with fibromyalgia [5, 6], and 5 million with chronic heart failure [7-9]), causing increased health cost and impaired quality of life.

In addition to numerous applications to exercise physiology and sports medicine [10], quantification of hemodynamic/metabolic parameters has potential to characterize disease status by monitoring abnormalities. Because functional impairments are not always apparent at rest, it is important to study hemodynamic and metabolic changes in response to stimulus [3, 8, 11-13]. For example, patients with peripheral arterial disease can exhibit normal resting blood pressures and flow, but impaired flow in following an exercise stress test [14]. Rhythmic exercise is an effective method for inducing changes in both BF and $\dot{V}O_2$. The ability to simultaneously monitor these parameters continuously and noninvasively during exercise has great potential for investigating muscle and exercise physiology, improving diagnosis and treatment assessment, as well as understanding pathophysiology of disease affecting skeletal muscle.

1.2 Blood Flow Measurement

There have been several previous efforts to monitor flow non-invasively, including Doppler ultrasound, laser Doppler, positron emission tomography (PET), and arterial-spin-labeled MRI (ASL-MRI) [15]. Doppler ultrasound is widely used, but is limited to imaging large vessels [16]. Flow through these vessels represents regional flow, which can obscure details found in evaluation of individual muscles [17, 18]. Laser Doppler is capable of monitoring flow in the small vessels of the microvasculature, but is incapable of penetrating to deep tissues, restricting measurement to shallow tissue (i.e. skin flow) [19]. PET [20] and ASL-MRI [21] are both capable of measuring flow in deep tissues, but require expensive and cumbersome equipment which can restrict the range of motion for exercise studies, and is often not practical for some laboratories or clinics. In

addition, most of these technologies are sensitive to muscle motion artifact, which can distort signals from contracting muscle. The limitations of these technologies have prevented widespread use in exercise research and clinical settings. The need exists, therefore, for a noninvasive technology capable of monitoring local deep tissue blood flow without the restriction imposed by large expensive equipment.

1.3 Blood Oxygenation Measurement

There are many different techniques for measuring blood oxygenation *in vivo*, including blood sampling for arterial blood gas tests (ABGs) [22], functional MRI (fMRI) [23], oxygen electrodes [24], spectroscopic techniques such as electron paramagnetic resonance (EPR), nuclear magnetic resonance (NMR) [25], and near-infrared spectroscopy (NIRS) tissue-oximetry [26]. Concentration of metabolites in blood that depend on the presence of oxygen can also be used to monitor oxygen levels, but is an indirect secondary measurement which is also invasive [25]. ABGs are invasive, and are generally reflective only of arterial blood oxygenation, not local tissue blood oxygenation or oxygen uptake. Oxygen electrodes are invasive and can only measure oxygen partial pressure (PO_2) in a tiny spot, and often produce inconsistent results in highly heterogeneous tissues. fMRI, EPR, and NMR are very expensive and cumbersome, and not frequently used in many clinical or research environments. By far the most popular method for measuring blood oxygenation is NIRS tissue-oximetry. NIRS allows for noninvasive measurement *in vivo*, and advances in technology have made NIRS monitors inexpensive, fast, portable, and easy to use.

1.4 Oxygen Consumption Rate ($\dot{V}O_2$) Measurement

Oxygen consumption in skeletal muscle has also been quantified by a variety of technologies. Spirometry measures whole body $\dot{V}O_2$, but does not provide information regarding the contributions of individual organs or tissues [27]. Muscle $\dot{V}O_2$ can be determined invasively using catheterization and blood sampling, with application of the Fick principle [28, 29]. Blood sampling is well-established, but aside from the invasiveness of the procedure, the data provided remain regional in scope of O_2 dynamics. Samples are usually taken from major vessels which perfuse groups of muscles, and do not assess dynamics at the level of the local microvasculature. 31-phosphorus magnetic resonance spectroscopy (^{31}P-MRS) is capable of monitoring local muscle oxygen kinetics, but requires expensive and cumbersome equipment which limits measurement during exercise, has limited sensitivity, and poor temporal resolution [30]. Thus, there is a need for a simple method to determine local muscle $\dot{V}O_2$ easily and noninvasively in exercising muscle.

1.5 Near-infrared Spectroscopy (NIRS)

Near-infrared (NIR) diffuse spectroscopic technologies for tissue hemodynamic monitoring have gained popularity in recent years, including many studies investigating muscle physiology [10, 31, 32]. NIR technology offers several attractive features making it ideal for research and clinical use, including noninvasiveness, portability, and inexpensiveness. NIR light is well-suited to biomedical applications due to the low absorption of tissue in the spectral (600 – 950 nm) window (see Figure 1) in biological tissues [33]. Reduced absorption allows for deep penetration of photons into the tissue of

interest. As they pass through the tissue, photons interact with scatterers (cell membranes, organelles, nuclei) and absorbers (deoxy- and oxy-hemoglobin, water). In a scattering event, light is redirected along a new path, and in an absorbing event, light intensity is attenuated. At wavelengths in the NIR range, scattering is much greater than absorption, and photons undergo diffusive motion as they are reflected back to the surface of the tissue. Tissue optical properties are characterized by absorption and reduced scattering coefficients, represented by μ_a and μ_s' (cm^{-1} units), respectively.

NIRS is typically categorized into three different techniques based on illumination type [34]. The continuous-wave (CW) paradigm uses constant illumination, and measures light attenuation through the tissue (see Figure 2a). The frequency domain (FD) paradigm uses intensity modulated light to illuminate the tissue, and measures both the attenuation and the phase shift at the detector (see Figure 2b). The time-domain (TD) paradigm is based on a pulse injection of light into the tissue, and the time-resolved measurement at the detector (see Figure 2c). The shape of the detected pulse following attenuation and broadening provides property information about the propagation tissue. Of the techniques, CW is the simplest and least expensive, but only provides relative values for deoxy-, oxy-, and total hemoglobin concentrations ([Hb], [HbO_2], and [tHb]). FD and TD techniques are capable of measuring absolute μ_a and μ_s', and thus absolute concentrations, but are also more expensive and technologically complex. In addition, the TD technique provides more spatial information about properties at differing depths, but at a cost to temporal resolution.

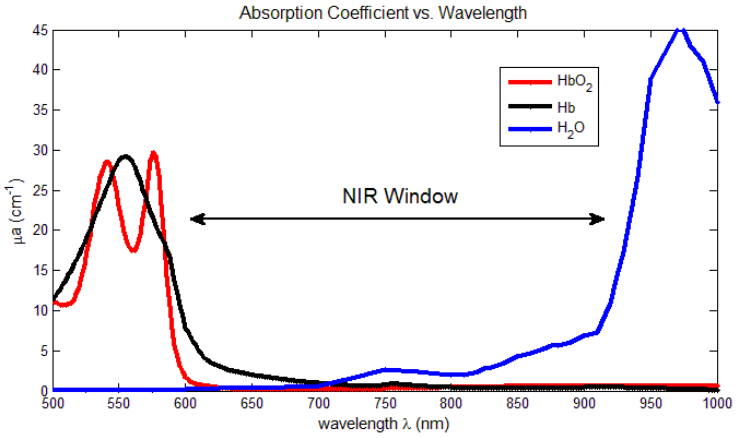

Figure 1. Absorption Spectra of Hemoglobin and Water

The absorption coefficients (μ_a) shown as a function of wavelength (λ) for oxygenated hemoglobin (HbO_2), deoxygenated hemoglobin (Hb), and water (H_2O). Within the NIR spectral window (~600 – 900 nm), light is able to penetrate deep tissue due to low absorption.

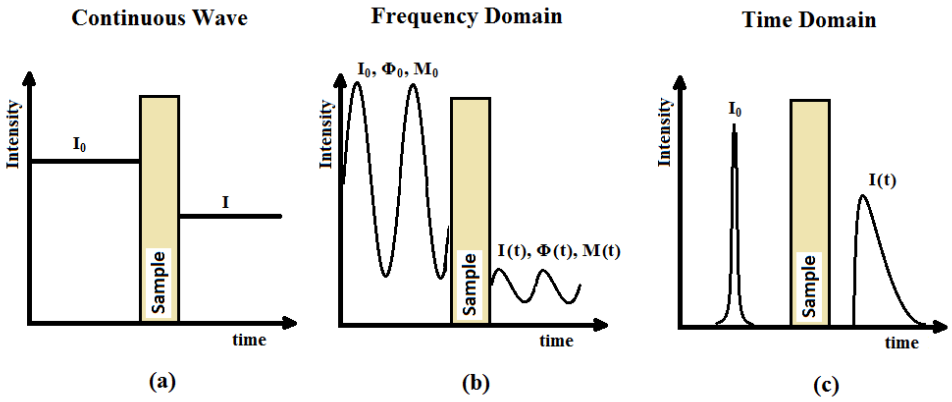

Figure 2. NIRS Modalities

Sample input and output intensity signals representing the three types of NIRS techniques. Panel (a) shows continuous wave (CW) spectroscopy, in which attenuated intensity of continuous illumination is monitored. Panel (b) shows frequency domain (FD) spectroscopy, in which input light is modulated and the amplitude attenuation and phase shifts are detected. Panel (c) shows time domain (TD) spectroscopy, in which an impulse of light is emitted into the tissue, and the intensity change with respect to time is detected. In the figure, I represent intensity, Φ represents phase, and M represents the frequency of modulation.

1.6 Diffuse Correlation Spectroscopy (DCS)

Diffuse correlation spectroscopy (DCS) is a relatively new technique for monitoring relative blood flow changes in deep tissues [33, 35, 36]. DCS takes advantage of the same optical window as traditional NIRS techniques, but employs a long-coherence NIR CW laser as the light source, and monitors speckle fluctuations at the tissue surface using photodetectors. Speckle fluctuations are caused by photon interactions with moving scatterers, primarily red blood cells (RBCs) in the microvasculature. Each scattering event causes a random scattering phase shift in the light field of the photons, and the superposition of multiple fields with different phases creates an interference pattern. The time-dependent light intensity fluctuations can be quantified by temporal autocorrelation functions.

DCS relative flow measurements are obtained by fitting experimentally obtained normalized temporal intensity autocorrelation functions from the speckle fluctuation to theoretical solutions based on the correlation diffusion equation, from which a blood flow index (BFI) is derived. Relative change in blood flow (rBF) can then be calculated by normalizing BFI to its baseline value (e.g. before physiological changes). DCS technology has many advantages, including noninvasiveness, portability, high temporal resolution, deep tissue penetration, and low running cost. All of these features make DCS an attractive option for clinical studies on even fragile patient populations, as well as research studies in the field.

DCS for rBF measurement has been applied to a wide variety of tissues, including human brain [37-42], head/neck tumor [43, 44], breast [45, 46], and muscle [47-49], and has been validated by a variety of local flow measurement techniques, including laser

Doppler [33, 50], Xenon-CT [39], and perfusion MRI (ASL-MRI) [33, 49]. In moving skeletal muscle, fiber motion during contraction can also cause scattering and introduce a motion artifact leading to overestimation of flow. This poses a significant problem for monitoring hemodynamics during physical activity [51]. Previous efforts to reduce motion artifact have required precise co-registration of signals with a dynamometer and off-line analysis [50].

1.7 Diffuse Optical Measurement Limitation and Current Study

It is apparent from review of literature, that there is a need for a simple method to noninvasively quantify local blood flow, blood oxygen saturation, and oxygen consumption in muscle during exercise without overly restricting movement. NIRS technology is capable of monitoring absolute oxygenation in tissue, and DCS technology is capable of directly monitoring relative blood flow (rBF) in muscle. Combining these two technologies, it is possible to derive relative oxygen consumption ($r\dot{V}O_2$) based on the Fick principle [13] (see Section 2.4). With such combination of multiple parameters, investigators and clinicians could be capable of obtaining a much clearer picture of muscle hemodynamics and metabolism.

Currently DCS-based measurements are limited to providing only relative information, as the flow index is calculated relative to the baseline. To overcome this limitation, it is necessary to employ some method of calibration. Absolute measurements of flow can be obtained readily with NIRS through venous occlusion protocols [1, 28, 52-54]. This technique has been validated against other modalities including the clinically accepted method of strain-gauge plethysmography. Although this method provides

absolute BF measurement, it requires interruption of natural flow response (as occlusions require ~10 s), which is not ideal for monitoring the rapid hemodynamic changes associated with exercise and recovery. Employing this protocol at rest determines an absolute baseline flow which can be used to calibrate the continuous relative DCS measurements. This eliminates the need for additional occlusions during exercise and allows for direct measurement of the natural flow response with higher temporal resolution. Similarly, the derived $r\dot{V}O_2$ signal can be calibrated through arterial occlusion [28, 55, 56]. Absolute $\dot{V}O_2$ measurement can be determined by monitoring the rate at which muscle converts oxy-hemoglobin (HbO_2) to deoxy-hemoglobin (Hb) while blood supply and return is occluded. The resting baseline absolute $\dot{V}O_2$ determined prior to exercise can then be used to calibrate the $r\dot{V}O_2$ signal from the hybrid instrument.

Muscle motion artifact presents another limitation preventing widespread application of DCS-based measurement techniques to exercise study. In order to overcome this limitation, it is necessary to employ a method which eliminates measurement while the muscle is contracting. To address this issue, a dynamometer based gating algorithm was embedded into the control software of a hybrid instrument (see Chapter 2.3). This algorithm uses signals generated by a dynamometer to determine the contraction status of muscle, and control data acquisition accordingly.

This study combines occlusive calibration protocols with gated NIRS/DCS measurements to investigate the feasibility of directly measuring absolute BF, S_tO_2, and $\dot{V}O_2$ in actively exercising skeletal muscle. This method was applied to dynamic exercise in the forearm flexor muscles of a nine young healthy subjects. Following validation of results in the young healthy population, the technique was applied to eleven fibromyalgia

patients and thirteen age-matched healthy controls to investigate differences in hemodynamic and metabolic responses to exercise.

This thesis is organized into the following chapters. Chapter 2 discusses the theory behind NIRS and DCS measurements, and describes the hybrid instrument and its data acquisition sequence. Chapter 3 describes the measurement protocol, beginning with an overview of procedure, followed by a more detailed description of each individual component. The details of the gating algorithm are also described. Chapter 4 describes the experimental procedures for the validation study in young healthy subjects. Chapter 5 details the application of the method to a fibromyalgia disease population (with age-matched healthy controls). Results are presented with accompanying discussion and critique in Chapter 6. Finally, Chapter 7 discusses the novel contributions of this work as well as directions for future research.

CHAPTER 2: THEORY

Measurements in this study were made using a hybrid NIR diffuse optical instrument which combined a commercial FD NIR tissue-oximeter (the Imagent from ISS, Inc., IL, USA) [57], and a custom-built NIR DCS flow-oximeter [58] (see Figure 3). These two devices communicate through control software in external computers to make concurrent measurements of tissue optical properties and blood flow indices, from which hemodynamic and metabolic parameters can be derived. Parameters were evaluated in a young healthy population, as well as a fibromyalgia patient population with age-matched healthy controls. This chapter is organized as follows. First, the theory behind FD NIRS measurement of tissue optical properties and chromophore concentration calculation is discussed in Chapter 2.1. Then the principles behind DCS measurement of blood flow indices are outlined in Chapter 2.2. The configuration of the hybrid instrument is described in Chapter 2.3. Finally, the derivation for $\dot{V}O_2$ measurement is described in Chapter 2.4.

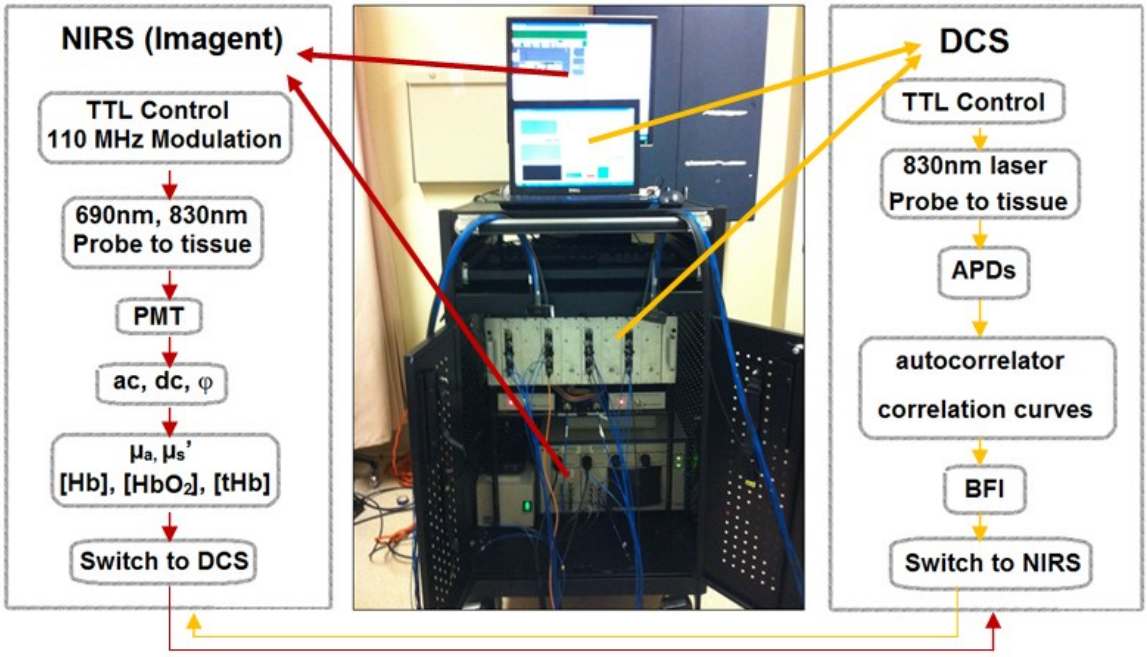

Figure 3. Hybrid Optical Instrument

The hybrid optical instrument combining a commercial Imagent (ISS, Inc.) FD spatially-resolved NIRS oximeter and the custom-built DCS instrument. The Imagent instrument includes 110 MHz modulated sources (of which the 690 and 830 nm wavelengths are used), photomultiplier tube (PMT), and desktop computer control, which ultimately calculates tissue optical properties (μ_a and μ_s') and deoxy-, oxy-, and total hemoglobin concentrations ([Hb], [HbO_2], and [tHb]). NIRS measures the modulated light amplitude (ac), average light intensity (dc), and phase (φ) of light at the detector. The DCS instrumentation includes an 830 nm laser source, avalanche photodiodes (APDs), autocorrelator board, and laptop computer control, which ultimately calculates the blood flow index (BFI). The two alternate measurements via triggers. Light is delivered through optical fibers to a black probe placed on the skin surface (see Figure 4).

2.1 NIRS for Oxygenation Measurement

A commercial 4-wavelength (690, 750, 780, and 830 nm) FD multi-distance spatially resolved spectroscopy instrument (Imagent, ISS) is employed to quantify μ_a, μ_s', [HbO_2], and [Hb] in muscle. Total hemoglobin concentration ([tHb]) is calculated as: [tHb] = [HbO_2] + [Hb], and tissue blood oxygen saturation (S_tO_2) is calculated as: $S_tO_2 = 100\% \cdot$

[HbO_2]/[tHb]. Parameters are measured using only the 690 and 830 nm wavelengths, modulated at 110 MHz. NIR light is delivered to the tissue via optical source fibers, and backscattered photons are collected by detector fibers located a few centimeters away. Source and detector fibers are embedded in a black flexible probe placed on the skin surface. Four source fibers per wavelength (8 total) are placed at distances of 2.0, 2.5, 3.0, and 3.5 cm from a detector fiber bundle (see Figure 4). The detector fibers are connected to a photomultiplier tube (PMT), which converts the light intensity to a voltage signal. From the detected light, changes in modulated light amplitude (ac), average light intensity (dc), and phase shift (φ) can be determined for each source-detector separation (r). Through solutions to a photon diffusion equation [57], μ_a and μ_s' can be derived from the detected light amplitude and phase shift (i.e., ac, dc, φ). For a semi-infinite geometry, it has been found that an approximate linear relationship exists between r and the logarithmic $ac \cdot r^2$, logarithmic $dc \cdot r^2$, or φ. These approximate relationships are described by the following equations [59] and adopted in the ISS Imagent instrument:

$$\ln\left(dc \cdot r^2\right) = rS_{dc}\left(\mu_a, \mu_s'\right) + In_{dc}\left(D, K_{dc}\right) \tag{1}$$

$$\text{where} \quad S_{dc} = -\left(\frac{\mu_a}{D}\right)^{1/2} \tag{2}$$

$$\varphi = rS_{\varphi}\left(\mu_a, \mu_s', \omega, v\right) + In_{\varphi}\left(K_{\varphi}\right) \tag{3}$$

$$\text{where} \quad S_{\varphi} = \left(\frac{\mu_a}{2D}\right)^{1/2}\left[\left(1+\left(\frac{\omega}{v\mu_a}\right)^2\right)^{1/2} - 1\right]^{1/2} \tag{4}$$

$$\ln\left(ac \cdot r^2\right) = rS_{ac}\left(\mu_a, \mu_s', \omega, v\right) + In_{ac}\left(D, K_{ac}\right) \tag{5}$$

$$\text{where} \quad S_{ac} = -\left(\frac{\mu_a}{D}\right)^{1/2}\left[\left(1+\left(\frac{\omega}{v\mu_a}\right)^2\right)^{1/2}+1\right]^{1/2} \tag{6}$$

where ω is the angular frequency of modulation, v is the speed of light in the medium, D is the photon diffusion constant ($D \approx 1/3\mu_s'$), K_φ is the relative phase of the source plus any phase shifts outside the sample, K_{ac} and K_{dc} are constants depending on detector sensitivity factors, modulation depth, and source intensity, and In_{dc}, In_φ, and In_{ac} are line intercepts from the multiple separation line fit. Only the slope of φ and any of $r^2 \cdot ac$ or $r^2 \cdot dc$ slope are necessary to obtain optical properties for each wavelength. The combination of S_{ac} and S_φ has the added advantage of reducing influence from background light [60]. The absorption coefficient can be decomposed into contributions from individual tissue chromophores by the following [33]:

$$\mu_a(\lambda) = \sum_i \varepsilon_i(\lambda)[i] \tag{7}$$

where $\varepsilon_i(\lambda)$ is the wavelength-dependent extinction coefficient for the i^{th} chromophore, and [i] is the concentration for the i^{th} chromophore, to be reconstructed.

During preliminary testing, data showed that the phase component of FD spatially resolved spectroscopy introduced too much noise for adequate slope fitting during BF calibration (see Section 3.2). Thus, only the amplitude differences from a single source-detector separation (2.0 cm) were used to calculate relative changes in chromophore concentration ($\Delta[HbO_2]$, $\Delta[Hb]$) based on the Beer-Lambert law [61], and added to absolute baselines (determined as the average of the first 10 data points).

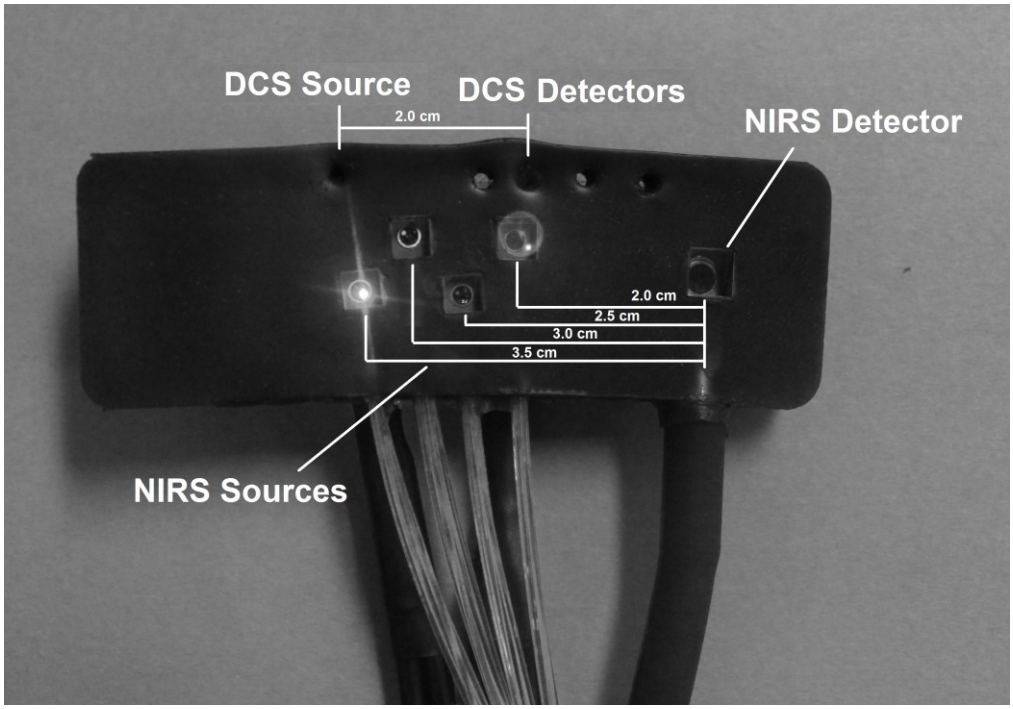

Figure 4. Hybrid Optical Probe

The configuration for the hybrid optical probe, embedded with source and detector fibers for both the Imagent NIRS and the DCS instruments. Probe is of black flexible silicon, and the surface shown is placed in direct contact with the skin surface.

2.2 DCS for Blood Flow Measurement

Diffuse correlation spectroscopy (DCS), also known as diffusing wave spectroscopy (DWS) [62], is an extension of the single scattering dynamic light scattering (DLS) technique to the multiple scattering limit [40]. In optically thick systems, such as biological tissue, light is scattered multiple times before being absorbed or leaving the sample. By accounting for multiple scattering events, DCS is able to probe and obtain information from deep tissues. Details regarding the complete theoretical development of DCS can be found elsewhere [63].

DCS uses a single CW laser (830 nm) with long coherence length (> 5 meter) to emit photons into the tissue through a multimode optical fiber embedded in the same black flexible probe as the FD NIRS fibers (see Figure 4). Four single-mode detector fibers at a specified distance away measure light speckle fluctuations at the surface caused by moving scatterers (primarily red blood cells). The photons are detected and counted by avalanche photodiodes (APDs, PerkinElmer Inc., Canada), and its output is fed to an autocorrelator board (correlator.com, NJ). The autocorrelator determines the normalized light intensity temporal autocorrelation function, $g_2(\mathbf{r},\tau)$ [40]:

$$g_2(\mathbf{r},\tau) = \frac{\langle I(t)I(t+\tau)\rangle}{\langle I(t)\rangle^2} \tag{8}$$

where $I(t)$ is the intensity at time t, the angular brackets denote temporal average, $\mathbf{r}$ is the general vector from the source to a point of detection, and τ is the delay time. The $g_2(\mathbf{r},\tau)$ functions from the four detectors are averaged together to improve the signal-to-noise ratio (SNR). The normalized intensity temporal autocorrelation function is then related to the normalized electric field autocorrelation function ($g_1(\mathbf{r},\tau)$) via the Siegert relationship [64]:

$$g_2(\mathbf{r},\tau) = 1 + \beta\left|g_1(\mathbf{r},\tau)\right|^2 \tag{9}$$

where β depends on laser stability, coherence length, and detection optics, and is inversely proportional to the number of speckles detected. β is determined experimentally for each measurement from the intercept of $g_2(\mathbf{r}, \tau)$ as $\tau \rightarrow 0$.

Light diffusion in highly scattering media is characterized by the correlation diffusion equation, which is rigorously derived elsewhere [35, 40, 63]:

$$\left(D\nabla^2 - v\left(\mu_a + \frac{1}{3}\alpha\mu_s' k_0^{\,2} < \Delta r^2(\tau) > \right) \right) G_1(\mathbf{r},\tau) = -vS_0(\mathbf{r}) \tag{10}$$

where $D \approx v/(3\mu_s')$ is the photon diffusion coefficient, v is the speed of light in the medium, $k_0 = 2\pi n/\lambda$ is the wavevector of photons in the medium, and $S_0(\mathbf{r})$ is the source-light distribution. The term $<\Delta r^2(\tau)>$ is the mean-square displacement of scatterers in time τ, and acts as an *effective* "absorption" term. In this equation, $G_1(\mathbf{r},\tau)$ is the *unnormalized* electric field autocorrelation function. The normalized electric field autocorrelation function is determined as $g_1(\mathbf{r},\tau) = G_1(\mathbf{r},\tau)/G_1(\mathbf{r},0)$. The homogenous CW solution to Eq. 10 for a semi-infinite geometry is:

$$G_1(\rho,\tau) = \frac{vS_0}{4\pi D}\left(\frac{e^{-K(\tau)r_1}}{r_1} - \frac{e^{-K(\tau)r_2}}{r_2} \right) \tag{11}$$

where ρ is the source-detector separation distance, S_0 is the source intensity, $K^2(\tau) = 3\mu_a\mu_s' + \mu_s'^2 k_0^{\,2}\alpha < \Delta r^2(\tau) >$, $r_1 = [\rho^2 + (z - z_0)^2]^{1/2}$, $r_2 = [\rho^2 + (z + z_0 + 2z_b)^2]^{1/2}$, $z_0 = 1/\mu_s'$, $z_b = 2(1 + R_{eff})/3\mu_s'(1 - R_{eff})$, $R_{eff} = -1.440n^{-2} + 0.710n^{-1} + 0.668 + 0.0636n$. R_{eff} accounts for the mismatch of refractive indices between air and the medium, with n as the ratio between them. For biological tissue, $n \approx 1.33$ [33]. For a semi-infinite geometry, the source is defined at position (0, 0, 0) and the detector at (ρ, 0, 0), with the tissue surface being in the $z = 0$ plane (see Figure 5).

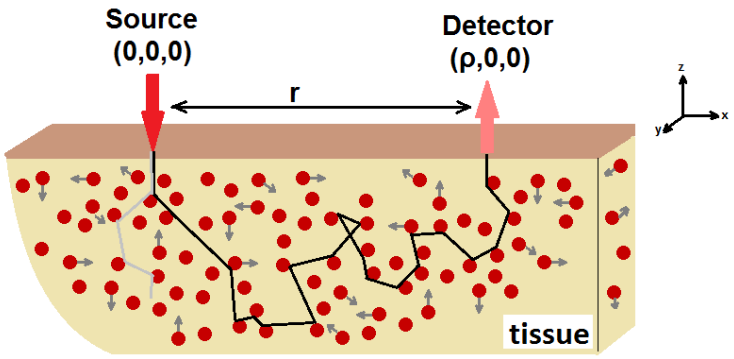

Figure 5. Tissue Absorption and Scattering

The source and detector placement on the tissue surface. Solid circles with gray arrows represent moving scatterers (RBCs). Black and light gray lines indicate potential photon paths.

The movement of dynamic scatterers in biological tissue is characterized by Brownian motion, $\langle \Delta r^2(\tau) \rangle = 6D_B\tau$, where D_B is the *effective* Brownian diffusion coefficient. The ratio of dynamic to total scatterers, α, is added to distinguish between moving and static scatterers. Combined, αD_B represents a blood flow index (BFI), which is used to determine relative blood flow (rBF) by comparison with the baseline resting BFI:

$$rBF = \frac{BFI}{BFI_{baseline}} \tag{12}$$

To quantify the BFI, first $g_2(\rho,\tau)$ is determined for a given sample time (~26 ms) from the autocorrelator board. This measurement is repeated multiple times within a given period (300 ms), and the $g_2(\rho,\tau)$ functions are averaged to achieve sufficient signal-to-noise ratio. The measured intensity autocorrelation curve is then transformed to the electric field autocorrelation curve, $g_1(\rho,\tau)$ via the Siegert relationship (**Eq. 9**). The experimental $g_1(\rho,\tau)$ is then fit with the theoretical solution of the correlation diffusion equation (**Eq. 10** and **Eq. 11**) by varying αD_B and using a least mean squares approach. The overall process of DCS measurement is shown in Figure 6.

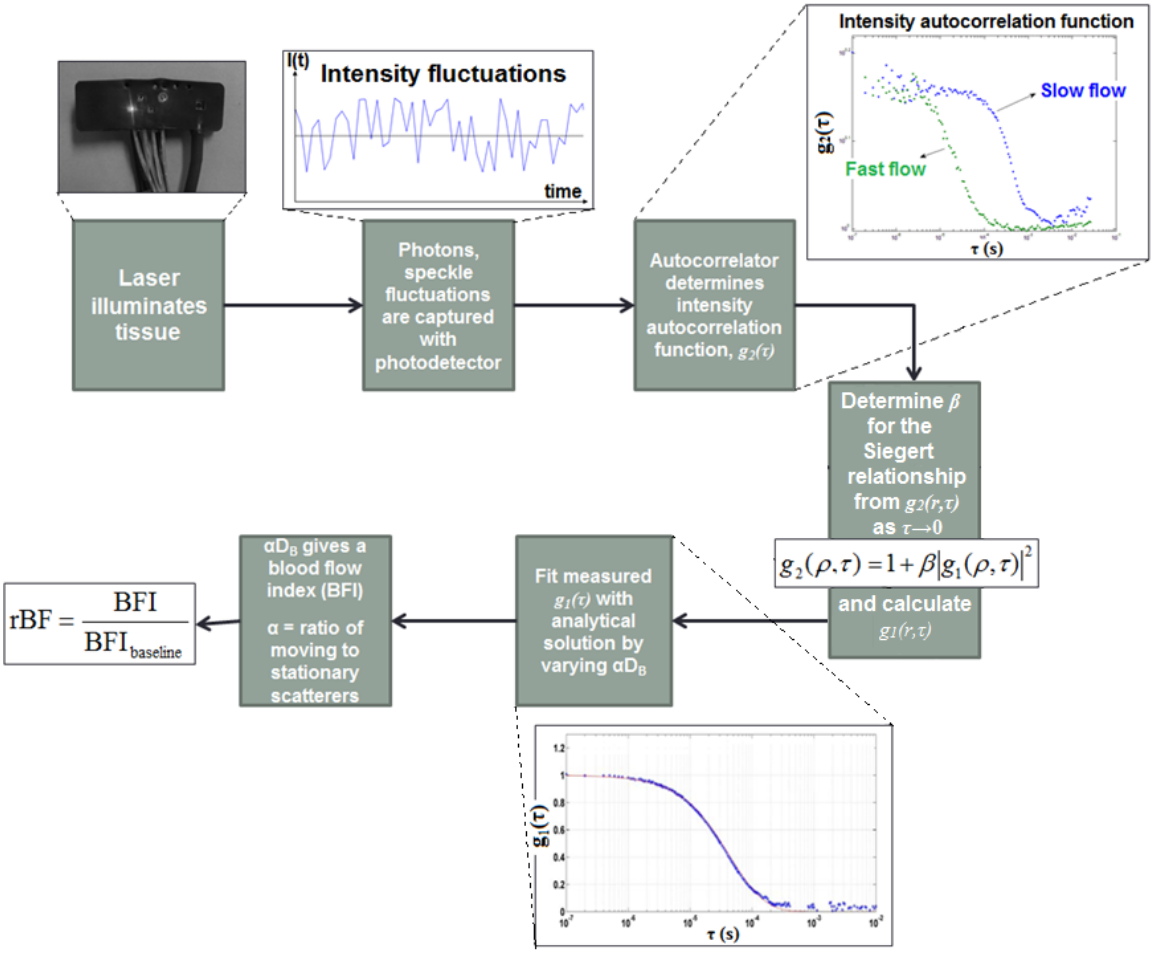

Figure 6. DCS Measurement and Analysis

A step-by-step guide to DCS measurement and analysis. First, the laser illuminates the tissue, and photon speckle fluctuations are captured with the APDs. The data are sent to an autocorrelator board, which calculates the temporal intensity autocorrelation function, $g_2(\tau)$. This is converted to the normalized temporal electric field autocorrelation function, $g_1(\tau)$, via the Siegert relationship. The measured $g_1(\tau)$ is then fit with the analytical solution by varying αD_B, which is also the blood flow index (BFI). From the BFI, rBF can be determined by normalizing to the baseline.

2.3 The Hybrid Instrument

The Imagent NIRS instrument and the DCS instrument were combined into a single hybrid device known as a hybrid tissue flow-oximeter (see Figure 3). This device has been described in detail elsewhere [58], and is capable of collecting data from either device individually or collectively by alternating sequentially between the two. When operating in tandem, a single acquisition sequence first begins with activation of the DCS laser, followed by data collection from the autocorrelator. The acquired data with individual autocorrelation functions is stored in a .dat file for later offline data analysis. The DCS laser is then deactivated, and notification is sent to the Imagent via a TTL trigger to begin NIRS data acquisition. NIRS acquisition begins with activation of a single 830 nm laser (4 in total) at a given source-detector separation (2.0, 2.5, 3.0 or 3.5 cm), followed by data collection from the PMT. Data collection iterates through sequential activation of each 830 nm laser (for a given source-detector separation). After data collection, the 830 laser is deactivated, and the sequence repeats for the 690 nm lasers. When a single round of data collection is completed for each laser at each separation, ac, dc, and phase data are stored in a .txt file. This .txt file can then later be analyzed by supplemental processing to calculate parameters such as μ_a and μ_s', which are saved in a user generated .log file. A control signal is then sent to the DCS to reinitiate the entire cycle. Data acquisition times are modifiable based on input parameters. Specific acquisition times for each protocol are detailed in the following chapters.

2.4 $\dot{V}O_2$ Derivation

To determine the absolute oxygen consumption rate ($\dot{V}O_2$) in exercising muscle, first the relative $\dot{V}O_2$ ($r\dot{V}O_2$) is calculated from tissue oxygen saturation (S_tO_2) measured by NIRS and rBF measured by DCS. Fick's Law states that $\dot{V}O_2$ is equal to the blood flow times the arterio-venous oxygen difference:

$$\dot{V}O_2 = BF \times ([O_2]_a - [O_2]_v) \tag{13}$$

where $[O_2]_a$ is the arterial oxygen concentration, and $[O_2]_v$ is the venous oxygen concentration. The percentage of oxygen extracted, or the oxygen extraction fraction (OEF) can be defined as: $OEF = ([O_2]_a - [O_2]_v)/[O_2]_a$. Combining this with the previous equation, $\dot{V}O_2$ can be defined by the following equation:

$$\dot{V}O_2 = OEF \times BF \times ([O_2])_a \tag{14}$$

Relative changes in each variable ($r\dot{V}O_2$, rOEF, rBF, $r[O_2]_a$) can be determined by dividing by the respective baseline value, so Eq. 14 becomes:

$$r\dot{V}O_2 = rOEF \times rBF \times (r[O_2]_a) \tag{15}$$

Making the assumption that $[O_2]_a$ does not change [13], the equation is reduced to:

$$rBF = rOEF \times rBF \tag{16}$$

OEF is related to tissue oxygen saturation by the following:

$$OEF = \frac{(S_aO_2 - S_tO_2)}{(\gamma \times S_aO_2)} \tag{17}$$

where S_aO_2 and S_tO_2 are arterial and tissue saturations, and γ is a measure of the percentage of blood volume contained in the venous compartment of the vascular system [65, 66]. For the duration of the measurement, γ is assumed to be constant (see Section

6.3). If S_aO_2 is also assumed to be a constant 100%, which has been found to be a reasonable approximation [13, 67], then Eq. 17 becomes:

$$\mathrm{rOEF} = \frac{(1 - S_tO_2)}{(1 - S_tO_{2\mathrm{baseline}})} \tag{18}$$

Substituting this into Eq. 16, $r\dot{V}O_2$ can be calculated as:

$$r\dot{V}O_2 = \mathrm{rBF}\frac{(1 - S_tO_2)}{(1 - S_tO_{2\mathrm{baseline}})} \tag{19}$$

S_tO_2 is measured directly with NIRS, and rBF is measured directly with the DCS, thus $r\dot{V}O_2$ can be measured by the hybrid instrument.

CHAPTER 3: MEASUREMENT PROTOCOL

The measurement protocol is divided into three distinct sub-protocols: venous occlusion for baseline absolute BF calculation, arterial occlusion for baseline absolute $\dot{V}O_2$ calculation, and the exercise protocol for modulation of BF, $\dot{V}O_2$, and S_tO_2. This chapter is divided as follows: First, there is an introduction to the overall measurement protocol in Chapter 3.1. Specifics of the calibration calculations are addressed in Chapter 3.2, and the exercise protocol is described in Chapter 3.3. Finally, the gating algorithm used during exercise is described in Chapter 3.4.

3.1 Measurement Protocol Overview

Following the methods detailed in previous work [1, 55, 68], three different protocols were used in this study to obtain absolute BF, S_tO_2, and $\dot{V}O_2$ in the forearm flexors during exercise. First, venous occlusion at 50 mmHg was applied on upper arm to obtain absolute baseline BF [1]. Second, arterial occlusion at 240 mmHg was applied to obtain absolute baseline $\dot{V}O_2$ [55]. Third, muscle BF and $\dot{V}O_2$ were manipulated by 5 minutes of rhythmic handgrip exercise at a fraction of the maximal voluntary contraction (MVC) [68] to test the capabilities of using the hybrid optical device for quantifying absolute BF and $\dot{V}O_2$ continuously during exercise. During all protocols, a black, flexible fiber-optic probe (see Figure 4) was taped to the skin surface above the forearm flexor muscles (flexor digitorum superficialis/profundus). This probe allowed for transmission of photons to the tissue via source fibers, and detection of backscattered photons at the tissue surface via detector fibers.

Before the optical probe was fixed, subjects were instructed to lie supine with the right arm extended, slightly elevated above heart level (< 20°). Elevation prevents pooling of the blood and facilitates venous return (see Figure 7). Elbow flexion was kept as close to 0° as possible. Resting blood pressure was obtained using an automatic monitor (Omron HEM-80, Kyoto), and skin/adipose tissue thickness at the probe site was measured with skinfold calipers (Lange 85300, TX).

First, individual MVC was determined for each subject by incremental isotonic handgrip exercise. Healthy subjects squeezed a handgrip device on a dynamometer (BTE PrimusRS, MD) through a distance of 5 cm for an increasing load until they were unable to perform the task. Initial load was set at ~20 N·m with an incremental increase of ~5 N·m. In most subjects, MVC could be determined within 4 contractions, minimizing the effect of fatigue or potentiation. Following MVC testing, the dynamometer load was reduced to a fraction of the MVC, and subjects completed a very brief training period (< 15 repetitions) to familiarize themselves with the contraction rhythm during the exercise protocol. A visual metronome on the dynamometer monitor aided subjects in keeping pace, and subjects were able to complete the exercise protocol at the set rhythm without difficulty. Subjects were then instructed to rest while the optical probe was taped to the right forearm and a fast-inflating automatic tourniquet cuff (Zimmer ATS 1000, IN) was placed on the right upper arm just above the elbow.

During the venous occlusion protocol, 1 minute baseline measurement was recorded, followed by three repetitions of 10 s occlusion (50 mmHg) separated with 30 s rest. For the arterial occlusion protocol, another 1 min baseline was recorded, followed by a 3-minute arterial occlusion (240 mmHg). Following the release of the arterial cuff, 5

minutes recovery data were collected to ensure hemodynamic recovery to baseline. After baseline had been reestablished, subjects performed 5 minutes handgrip exercise following the rhythm described above. Five minutes recovery data were then recorded. Data acquisition parameters and protocols are discussed in detail in the following sections.

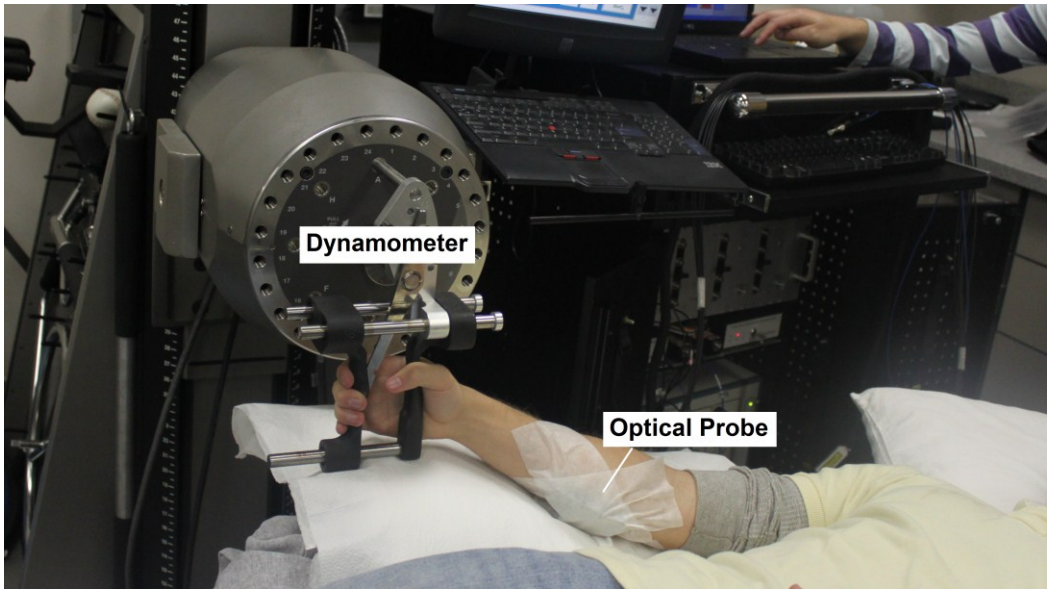

Figure 7. Arm Positioning and Probe Fixation during Protocol

During all protocols, subject was supine with the right arm extended slightly elevated above heart level (< 20°) to prevent pooling and facilitate venous return. The hand maintained the grip position, around the dynamometer attachment. The hybrid optical probe (see Figure 4) was taped to the forearm flexor muscles (flexor digitorum superficialis/profundus) following MVC test, prior to occlusions.

3.2 Calibration of Relative Signals with Absolute Baseline BF and $\dot{V}O_2$

The relative blood flow (rBF) signal acquired from the DCS was calibrated in this study by using venous occlusion in conjunction with NIRS measurement. Venous occlusion plethysmography is a widely accepted method for determining peripheral blood flow [15, 69], and has been used frequently in recent years with NIRS techniques [1, 28, 53, 70]. This technique has been applied on both resting and exercising muscle, and has been validated against the more conventional standard of strain-gauge plethysmography [1, 28]. During venous occlusion, a fast-inflating tourniquet cuff is applied to the upper arm just above the elbow and inflated to a pressure greater than the venous pressure, but lower than diastolic arterial pressure. Pressure between 30 – 60 mmHg gives the most reproducible results [71], and the most common convention is to use 50 mmHg (used in this study). By inflating the cuff to this pressure, venous outflow is occluded while arterial inflow is permitted, causing a total blood volume increase in the arm. This is recorded by NIRS measurements as an increase in [tHb] (see Figure 8). The initial rate of increase (~5 s) is directly proportional to the arterial inflow. BF is calculated by the following equation [72]:

$$\mathrm{BF} = \frac{1}{\mathrm{C}} \cdot \frac{d[\mathrm{tHb}]}{dt} \tag{20}$$

where C is the hemoglobin concentration of whole blood. In this study, a standard value of 14.1 g/dL [73] was used for C, but individual concentrations may be measured invasively through blood samples, obtained from patient records, or measured noninvasively via pulse CO-oximetry (Masimo, Inc., CA) [74]. [tHb] is converted from molar concentration to blood volume by multiplying by the molecular weight of

hemoglobin (64,458 g/mol) [75], and dividing by C. Absolute BF is expressed in units of ml blood per 100 ml tissue per minute [ml/100 ml/min].

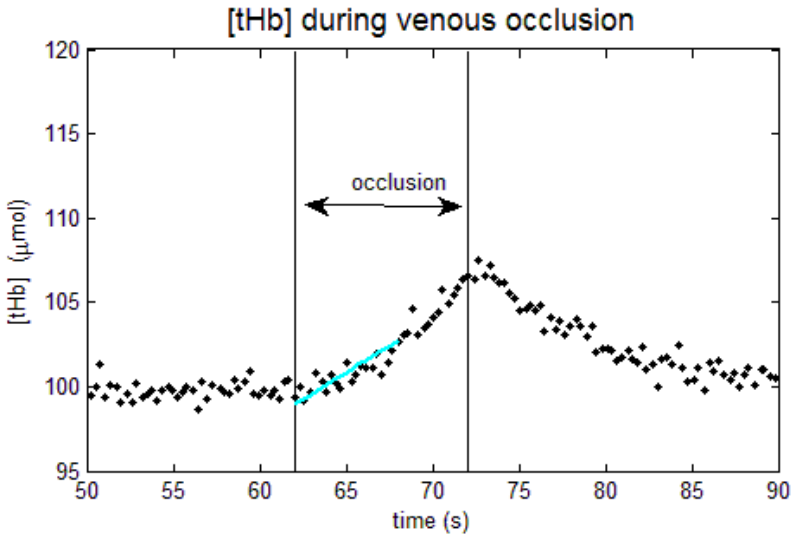

Figure 8. Slope Fitting during Venous Occlusion for Absolute BF Calculation

The [tHb] increase induced by 50 mmHg venous occlusion is fit with linear regression. The initial slope of the fitted line (~5 s) is indicative of the muscle BF (see Eq. 20). Vertical lines indicate application and release of venous pressure.

During the venous occlusion protocol, only NIRS data (without DCS) were collected at a sampling rate of 3.7 Hz. Only amplitude data were used in order to eliminate noise contributed by the phase component of the acquired data (see Section 2.1). Preliminary testing showed that this high sampling rate was adequate to precisely fit the [tHb] curve during venous occlusion measurements. One minute of baseline data were recorded prior to any venous occlusion. After baseline data acquisition, three venous occlusions were performed for 10 s each, with 30 s rest between each occlusion, and a 30 s recovery

period following the last occlusion. The baseline BF was then determined by averaging the three venous occlusion measurements.

Relative $\dot{V}O_2$ ($r\dot{V}O_2$, derived in Section 2.4) was calibrated in this study by observing the rate of oxygen desaturation ($[HbO_2] - [Hb]$) during the first 60 s of arterial occlusion [55]. During arterial occlusion, a fast-inflating tourniquet cuff is applied to the upper arm just above the elbow and inflated to a pressure significantly greater than systolic arterial pressure (240 mmHg used in this study). This maneuver causes a total interruption of the blood supply (i.e. oxygen supply), while the tissue continues to consume oxygen. $\dot{V}O_2$ is then proportional to the rate of oxygen desaturation ($[HbO_2] - [Hb]$), measured by NIRS (see Figure 9). Molar concentration of hemoglobin is converted to O_2 volume by multiplying by the O_2 molecular weight (32 g/mol) and the ratio of O_2 to hemoglobin (4:1), and dividing by the O_2 density (1.429 g/L). Tissue volume is converted to mass by dividing by the muscle density (1.04 kg/L) [53]. $\dot{V}O_2$ is then expressed as ml O_2 per 100 g muscle per minute [ml O_2/100 g/min].

For the arterial occlusion protocol, alternating NIRS measurements were combined with DCS measurements. While not used directly to calculate baseline $\dot{V}O_2$, DCS measurements provided validation that BF was adequately occluded. DCS sampling time was ~300 ms while NIRS sampling time was ~400 ms (~700 ms total sampling time per data point). The arterial occlusion protocol consisted of 1 minute resting baseline data, followed by a 3-minute arterial occlusion. Only the first 60 s of the desaturation during occlusion was fit to determine baseline $\dot{V}O_2$ (see Figure 9). Following release of the tourniquet, 5 minutes of resting recovery data were recorded.

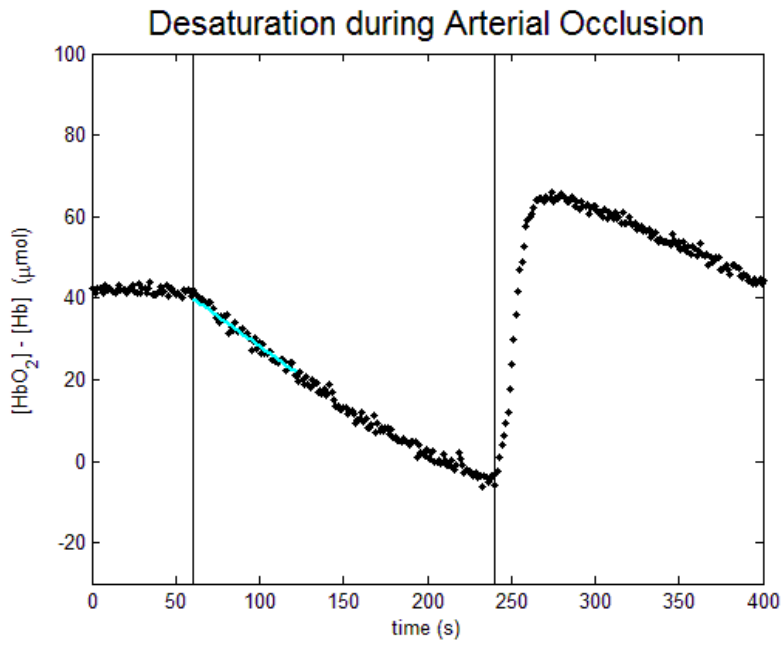

Figure 9. Slope Fitting during Arterial Occlusion for Absolute $\dot{V}O_2$ Calculation

The saturation decrease induced by 240 mmHg arterial occlusion is fit with linear regression. The slope of the fitted line during the first 60 s of occlusion is indicative of the muscle $\dot{V}O_2$. Vertical lines indicate application and release of arterial pressure.

3.3 Exercise Protocol

Following the release of the tourniquet and 5 minutes recovery from the arterial occlusion protocol, the software gating algorithm was engaged (see Section 3.4), and young healthy subjects (n = 9) were instructed to perform 5 minutes of handgrip exercise at 25% MVC (6.8 ± 0.6 N·m) at a rate of 1s contraction (~0.5 s to contract, ~0.5 s to release) followed by 1 s rest. At this submaximal exercise intensity, muscle is sufficiently challenged to reach a plateau $BF/\dot{V}O_2/S_tO_2$ without inducing obvious post-exercise hyperemic response [68]. This exercise protocol is in line with many other similar studies [1, 76, 77] to allow a basis for comparison of results. Each subject therefore performed 150 contraction cycles. Data were acquired during the relaxation

phase of exercise. Sampling times were the same as used for the arterial occlusion protocol (~300 ms DCS, ~400 ms NIRS, for ~700 ms total). Following exercise, the gating algorithm was disengaged, and 5 minutes of recovery kinetics were recorded.

For the fibromyalgia subjects (n = 11) and their healthy control counterparts (n = 13), a modified exercise protocol was used. Differing from the exercise protocol described above, dynamic exercise for these subject populations was performed at 50% MVC, at a rate of 15 contractions/minute (1 s contract, 1 s release, 2 s rest for each contraction cycle). Preliminary testing in 3 subjects in this older subject population showed that the slower rhythm of this contraction cycle was easier to follow than the 30 contractions/minute rhythm used in the young healthy population. To account for the slower cycle, the delay time used in the gating algorithm was 100 ms. Other data acquisition times were the same as that described in the preceding sections.

3.4 Embedded Gating Algorithm to Reduce Motion Artifact

Previous work in the field of diffuse correlation spectroscopy (DCS) has been limited by the fact that muscle contraction produces a signal artifact which can significantly overestimate flow [50]. To eliminate this motion artifact, a gating algorithm was embedded into the DCS data acquisition control software. This algorithm read analog voltage output signals from the dynamometer to determine periods of contraction and relaxation in the rhythmic exercise cycle. Once the output voltage exceeded a specified threshold indicating the transition from contraction (low voltage) to relaxation (high voltage), a trigger was initiated. The trigger allowed for a short delay (50 ms, specified by user) to account for any residual motion, then initiated data acquisition. After a frame

of data was recorded and stored, the software waited for the next rising edge in the dynamometer signal to reinitiate measurement. Input and control signals for the gating algorithm are shown in Figure 10.

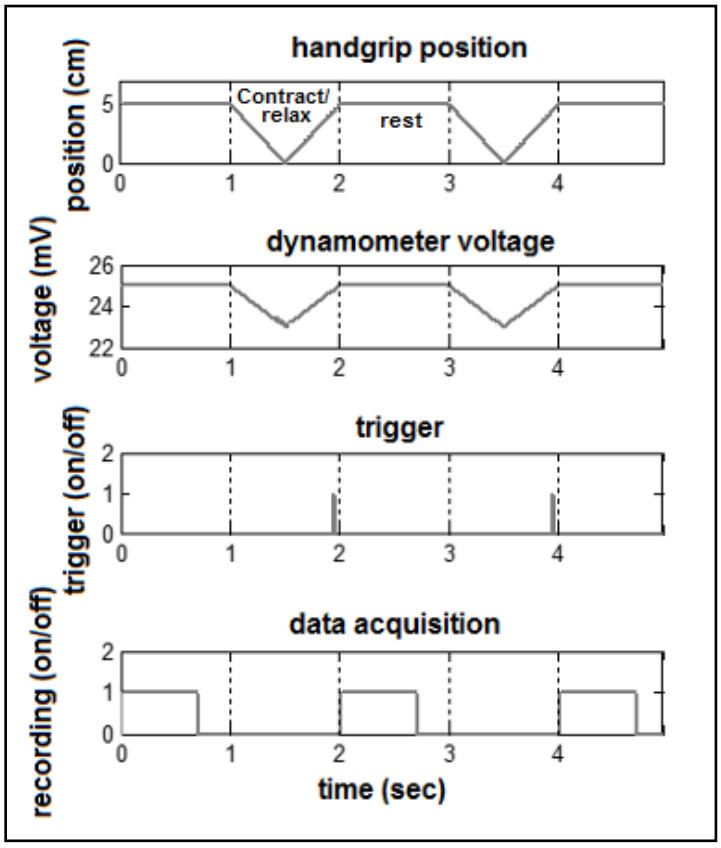

Figure 10. Input and Control Signals for Gating Algorithm

The output signals from the dynamometer and the software-generated signals that control the gating algorithm are shown. The *dynamometer voltage* mirrors the *handgrip position*, indicating contraction status of the muscle. Once the *dynamometer voltage* passes a threshold on the rising edge, the algorithm generates a *trigger* signal, which injects a small delay (to account for residual muscle tension/contraction) before initiating *data acquisition*. Data acquisition occurs between contractions, while the muscle is at rest. Following a data acquisition sequence, the algorithm pauses, waiting for the next rising edge in the *dynamometer voltage*.

CHAPTER 4: VALIDATION IN YOUNG HEALTHY SUBJECTS

The measurement protocol developed in this study was first used in a young healthy population and validated against previous literature results. Presentation of the results is ordered in the following manner. First, the physical characteristics of the population are described in Chapter 4.1. The effect of the embedded gating algorithm is then evaluated in Chapter 4.2. Next, the typical individual hemodynamic/metabolic response during the course of the entire measurement protocol is presented in Chapter 4.3, as well as the average results of BF, $\dot{V}O_2$, and S_tO_2 for all subjects during exercise in Chapter 4.4.

4.1 Young Healthy Subject Physical Characteristics

Nine healthy subjects (5 males, 4 females) volunteered to participate in this study following written consent in accordance with the University of Kentucky Institutional Review Board guidelines. Physical characteristics for the sample population were (mean ± SE) age 24.6 ± 0.6 yr, height 167.9 ± 2.5 cm, and weight 73.8 ± 8.2 kg (BMI 22.9 ± 3.2). Resting systolic arterial pressure was 116.2 ± 3.1 mmHg, skin/adipose tissue thickness (ATT) was 1.5 ± 0.2 mm, and MVC was 27.3 ± 0.6 N·m.

4.2 Effect of Gating Algorithm on Motion Artifact

Preliminary experimentation showed that the software gating algorithm was effective in removing a majority of the noise associated with motion artifact. Figure 11 shows DCS flow index (αD_B) raw signals acquired during exercise both without (Figure 11a), and with (Figure 11b) the gating algorithm. The two trials were performed on the same subject, at the same rate and intensity (25% MVC) as the exercise protocol for young

healthy subjects detailed in Section 3.3. The trials were separated by several minutes (> 6 minutes) to ensure BF and oxygenation recovery to baseline. The results clearly demonstrate the efficacy of the algorithm at removing noise due to motion artifact from the raw data signal.

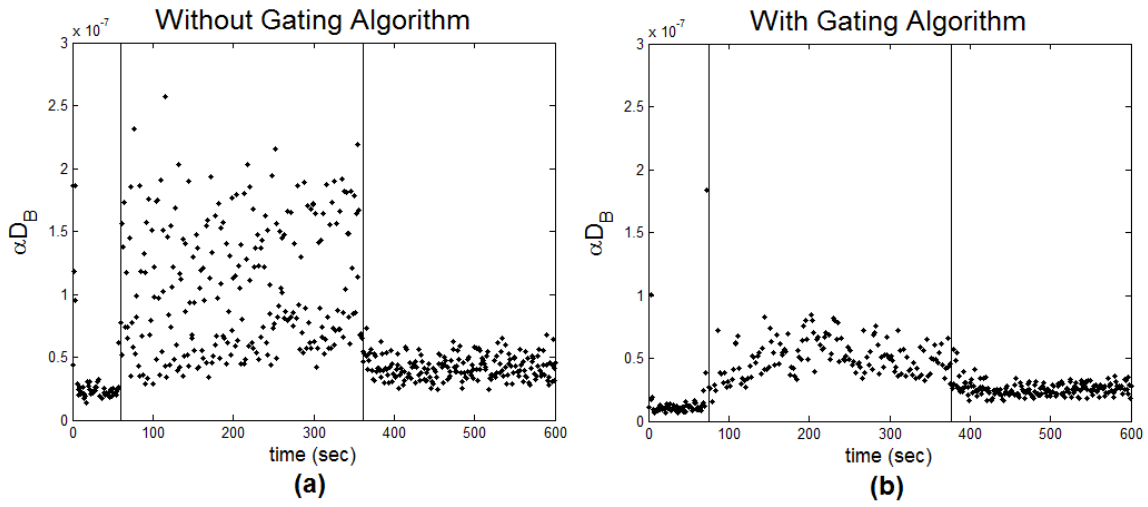

Figure 11. Motion Artifact Reduction with Application of Gating Algorithm

Raw DCS data acquired during exercise protocol (see Section 3.3). Panel (a) shows data collected without the gating algorithm running. Panel (b) shows data collected with the application of the algorithm. Raw data are presented as αD_B, the blood flow index. The vertical lines indicate the beginning and end of the exercise protocol.

4.3 Typical Individual Response

The typical muscle hemodynamic response for the entire protocol is shown for a single subject in Figure 12. Vertical lines denote the beginning and ending of physiological manipulations (occlusions, exercise). Dark bold lines superimposed on the data signals indicate slope fitting during both venous and arterial occlusions. During the venous

occlusions (VO), [tHb] increased at a rate proportional to the arterial inflow (see Section 3.2). Baseline BF for this subject obtained from the three venous occlusions was 2.48 ± 1.14 ml/100 ml/min. During arterial occlusion (AO), [tHb] remained constant, while the desaturation ($[HbO_2]$ – [Hb]) decreased at a rate proportional to $\dot{V}O_2$ (see Section 3.2). Correspondingly, there was a noticeable decrease in tissue oxygen saturation (S_tO_2), and the rBF signal from the DCS decreased to near zero. Baseline $\dot{V}O_2$ obtained from arterial occlusion was 0.11 ml O_2/100 g/min (5.04 μmol O_2/100 g/min). During the exercise protocol, $\dot{V}O_2$ increased, corresponding to a decrease in S_tO_2, and an increase in rBF to satisfy the metabolic demand. The absolute BF, $\dot{V}O_2$, and S_tO_2 during exercise are shown in Figures 13, 14, and 15 for the same subject.

4.4 Average Population Response

All subjects demonstrated similar trends during occlusion and exercise. Resting baseline BF for the 9 subjects (mean ± SE) obtained via venous occlusion was 1.76 ± 0.40 ml/100 ml/min. Baseline $\dot{V}O_2$ obtained by arterial occlusion was 0.12 ± 0.02 ml O_2/100 g/min (5.62 ± 1.03 μmol O_2/100 g/min), and baseline S_tO_2 was 68.0 ± 1.0%. To clearly see the general response to exercise, the filtered BF, $\dot{V}O_2$, and S_tO_2 signals were averaged across the subject population at 10 s time intervals throughout the protocol. The averaged exercise data are shown in Figures 16, 17, and 18. Pre-exercise BF value was 1.76 ± 0.42 ml/100 ml/min, determined as the average of data points 30 s before the beginning of exercise. This pre-exercise BF does not differ significantly from resting BF, indicating that there was no residual hyperemic response from arterial occlusion. Pre-exercise $\dot{V}O_2$ value was 0.11 ± 0.03 ml O_2/100 g/min, the same as the average resting

baseline value, and pre-exercise S_tO_2 value was 71.9 ± 1.9%. During exercise, BF increased rapidly during the first few minutes, then increased following a more exponential pattern to a gradual plateau. The $\dot{V}O_2$ dynamics during exercise mirrored this response with initial linear increase followed by exponential increase to a gradual plateau. Plateau values were determined as the average of data points 30 s before the end of exercise. For the 9 subjects, average plateau BF was 8.93 ± 2.81 ml/100 ml/min, plateau $\dot{V}O_2$ was 0.57 ± 0.13 ml O_2/100 g/min, and plateau S_tO_2 was 64.0 ± 2.2%.

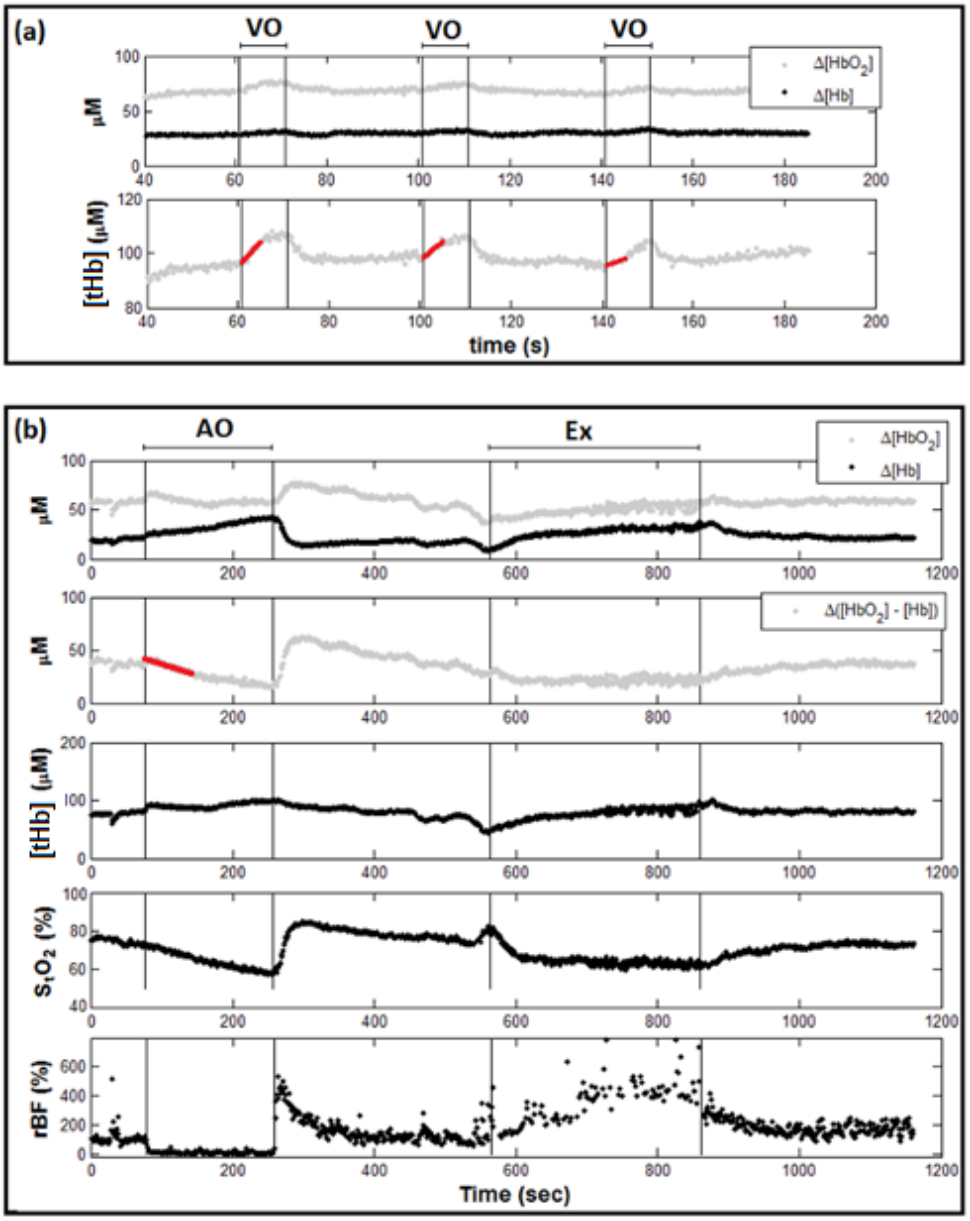

Figure 12. Hemodynamic Response in a Single Subject during Entire Protocol

Data collected for a single subject for the entire measurement protocol. Panel (a) shows [HbO_2], [Hb], and [tHb] response during three 50 mmHg venous occlusions (VO). The vertical lines denote the beginning and end of each occlusion. Panel (b) shows [HbO_2], [Hb], [tHb], desaturation ([HbO_2] – [Hb]), S_tO_2, and rBF responses during arterial occlusion (AO) and exercise (Ex). The pairs of vertical lines denote the beginning and end of AO and Ex.

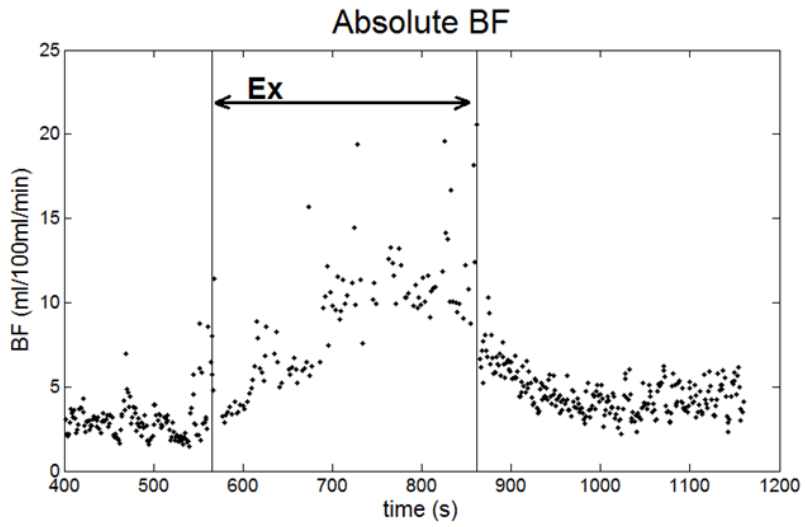

Figure 13. Absolute BF Response during Exercise in a Single Subject

The absolute BF response in an individual subject during exercise. The vertical lines denote the beginning and end of exercise. Residual noise prior to exercise may be caused due to involuntary muscle contractions in preparation for physical activity before the gating algorithm had been initiated.

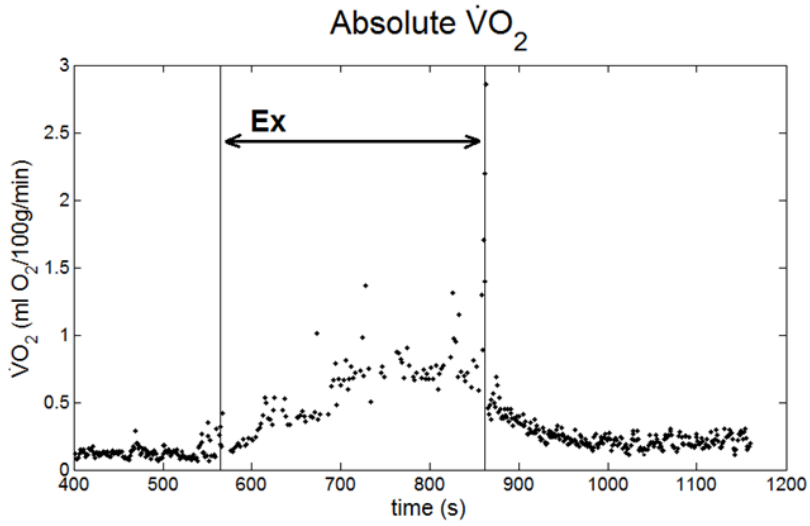

Figure 14. Absolute $\dot{V}O_2$ Response during Exercise in a Single Subject

The absolute $\dot{V}O_2$ response in an individual subject during exercise. The vertical lines denote the beginning and end of exercise. Residual noise prior to exercise may be caused due to involuntary muscle contractions in preparation for physical activity before the gating algorithm had been initiated.

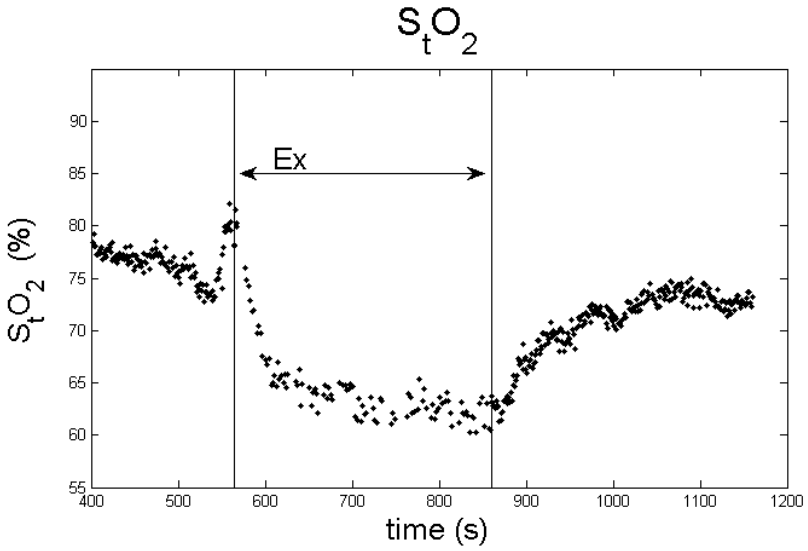

Figure 15. S_tO_2 Response during Exercise in a Single Subject

The S_tO_2 response in an individual subject during exercise. The vertical lines denote the beginning and end of exercise. The slight increase in S_tO_2 prior to exercise may be caused by increased flow from involuntary muscle contractions in anticipation to exercise, before oxygen demand increased.

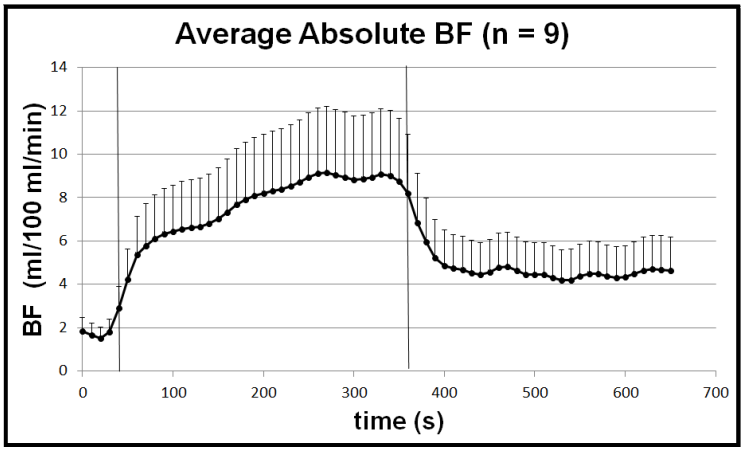

Figure 16. Average Population Absolute BF Response during Exercise

The average absolute BF response of 9 healthy young subjects during exercise. For clarity, data were filtered and averaged at 10 s time intervals. The vertical lines denote the beginning and end of exercise. Average pre-exercise BF value was 1.76 ± 0.42 ml/100 ml/min, determined as the average of data points 30 s before onset of exercise. Plateau BF value was determined as the average of data points 30 s before the end of exercise. For the 9 subjects, average plateau BF was 8.93 ± 2.81 ml/100 ml/min.

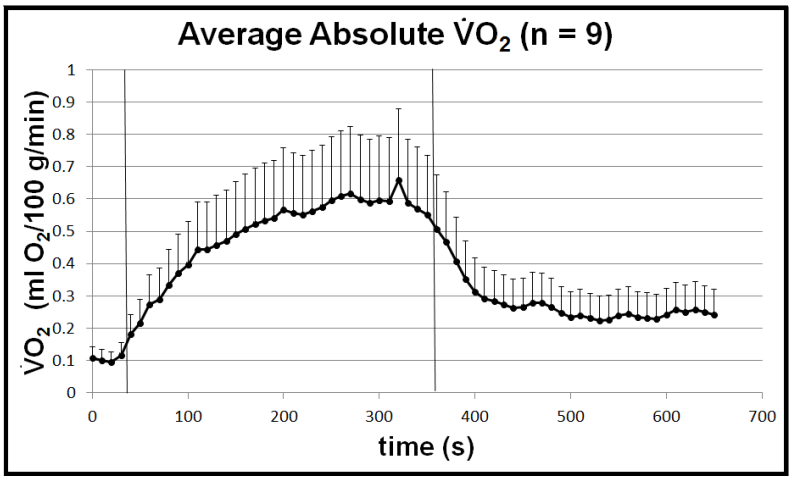

Figure 17. Average Population Absolute $\dot{V}O_2$ Response during Exercise

The average absolute $\dot{V}O_2$ response of 9 healthy young subjects during exercise. For clarity, data were filtered and averaged at 10 s time intervals. The vertical lines denote the beginning and end of exercise. Average pre-exercise $\dot{V}O_2$ value was 0.11 ± 0.03 ml O_2/100 g/min, determined as the average of data points 30 s before onset of exercise. Plateau $\dot{V}O_2$ value was determined as the average of data points 30 s before the end of exercise. For the 9 subjects, average plateau $\dot{V}O_2$ was 0.57 ± 0.13 ml O_2/100 g/min.

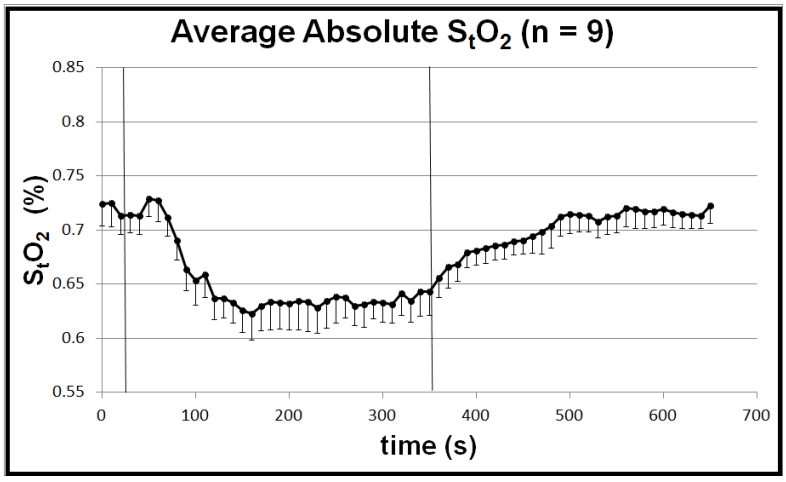

Figure 18. Average Population S_tO_2 Response during Exercise

The average S_tO_2 response of 9 healthy young subjects during exercise. For clarity, data were filtered and averaged at 10 s time intervals. The vertical lines denote the beginning and end of exercise. Average pre-exercise S_tO_2 value was 71.9 ± 1.9%, determined as the average of data points 30 s before onset of exercise. Plateau S_tO_2 value was determined as the average of data points 30 s before the end of exercise. For the 9 subjects, average plateau S_tO_2 was 64.0 ± 2.2%.

CHAPTER 5: APPLICATION TO DISEASE POPULATION

Chapter 5 outlines the application of the developed technique to investigation of fibromyalgia, a clinical disease of unknown etiology. Both subjects diagnosed with fibromyalgia, as well as age-matched healthy controls were investigated. The chapter opens with a review of the disease, and studies that have previously assessed flow and metabolism in affected populations in Chapter 5.1. The subject population demographics are then detailed in Chapter 5.2, and the results are presented in Chapter 5.3.

5.1 Hemodynamics and Metabolism in Fibromyalgia

Fibromyalgia (FM) is a chronic pain syndrome, characterized by widespread muscle pain and stiffness, aching, and fatigue. FM has been generally described as musculoskeletal pain in the absence of other apparent organic disease [78], and in 1990 the American College of Rheumatology committee established diagnosis criteria including history of widespread pain, and tenderness to digital palpitation at 11 of 18 specified tender sites [79]. FM affects approximately 2% of the U.S. population, and is approximately 7 times more prevalent in women than in men [80]. The pathophysiology of FM is unknown, but likely involves neurological, neuroendocrine, musculoskeletal, and psychological components [81].

FM treatments tend to be only partially effective, and target symptomatic relief, rather than the underlying cause. Therapies include pharmacological management [6], as well as exercise [82], hyberbaric oxygen therapy [83], and nitric oxide stimulants [84]. A commonality among partially effective treatments is a vasodilatory effect. This, in

addition to the qualitative description of FM pain as being similar to pain in muscles following heavy exercise or anaerobic metabolism, has led to the hypothesis that the pain of FM may be caused in part by vasomotor dysregulation or metabolic abnormality [84].

Although challenged, several studies have found apparent impairments in BF [5, 85-90] and metabolism [91-95] of FM subjects. These studies have independently explored hemodynamic/metabolic parameters using Doppler ultrasound [5], laser Doppler [86, 90], biopsy [85, 89, 91, 92], dynamic fluorescence videomicroscopy [87], laser fluxmetry [88], electrodes [93], and ^{31}P-MRS [95]. While some studies have used these methods in combination to investigate BF and metabolism in resting muscle [86, 89], no studies have yet been able to concurrently monitor BF, $\dot{V}O_2$, and S_tO_2 noninvasively during exercise in skeletal muscle of FM subjects.

The ability to monitor multiple hemodynamic and metabolic parameters simultaneously in response to exercise stimulus may open research options and have the potential to help elucidate the underlying mechanisms in FM and thus lead to more effective methods of treatment. Using the method developed in this thesis, eleven women diagnosed with FM and thirteen age-matched healthy controls were monitored for BF, $\dot{V}O_2$, and S_tO_2 changes during 50% MVC dynamic handgrip exercise.

5.2 Physical Characteristics of Subjects

Initially, eleven subjects diagnosed with FM and thirteen age-matched healthy controls (HC) were voluntarily recruited to participate in this study following written consent in approval with the University of Kentucky Institutional Review Board guidelines. One FM subject recruited for evaluation was excluded from data analysis due to excessive

ATT thickness (10 mm) which affected light penetration into the muscle. Therefore, data are presented for only 10 subjects. Only female subjects were recruited for this study. Physical characteristics for the sample population (mean ± SE) are given in Table 1. In all parameters except MVC, no significant differences were found between populations. The MVC for HC subjects was slightly lower than that for young healthy subjects, while the MVC of FM subjects was significantly lower than both healthy populations.

Table 1. Physical Characteristics of Fibromyalgia (FM) Subjects and Age-Matched Healthy Controls (HCs)

Parameter	HC (n = 13)	FM (n = 10)	p-value (Student's t-test)
Age (yrs)	57 ± 1.2	60 ± 2.3	0.2163
BMI	25.1 ± 0.8	24.4 ± 1.1	0.5849
Syst. BP (mmHg)	123.7 ± 3.9	125.4 ± 3.1	0.7354
ATT (mm)	2.9 ± 0.4	2.9 ± 0.4	0.9945
MVC (N·m)	24.14 ± 0.84	15.31 ± 1.23	<0.0001*

5.3 Typical Individual Response

The typical muscle hemodynamic/metabolic response for the exercise protocol is shown for a single HC and FM subject in Figures 19, 20, and 21. Vertical lines denote the onset and end of exercise. Pre-exercise BF, measured as the average of points 30 s before the onset of exercise was 1.60 and 1.62 ml/100 ml/min for the HC and FM subjects, respectively. Pre-exercise $\dot{V}O_2$ was 0.03 and 0.04 ml O_2/100 g/min, and pre-exercise S_tO_2 was 70.1 and 72.3%. Plateau BF, measured as the average of points 30 s before the end of exercise was 10.88 and 3.16 ml/100 ml/min for HC and FM subjects respectively, while plateau $\dot{V}O_2$ was 0.30 and 0.12 ml O_2/100 g/min, and S_tO_2 was 59.9 and 68.7%. During the exercise protocol, $\dot{V}O_2$ increased, corresponding to a decrease in S_tO_2, and an increase in BF to satisfy the metabolic demand.

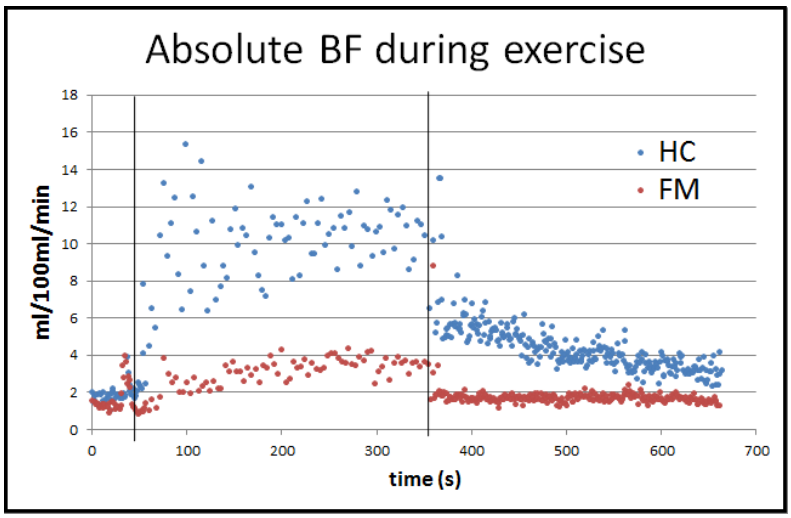

Figure 19. Individual HC and FM BF Response to Exercise

Raw absolute BF data in response to exercise for both a single HC subject and FM subject are shown. Vertical lines indicate the beginning and end of exercise. Pre-exercise BF value was 1.60 ml/100 ml/min for the HC subject and 1.62 ml/100 ml/min for the FM subject. Plateau BF values were 10.88 and 3.16 ml/100 ml/min for the HC and FM subjects, respectively.

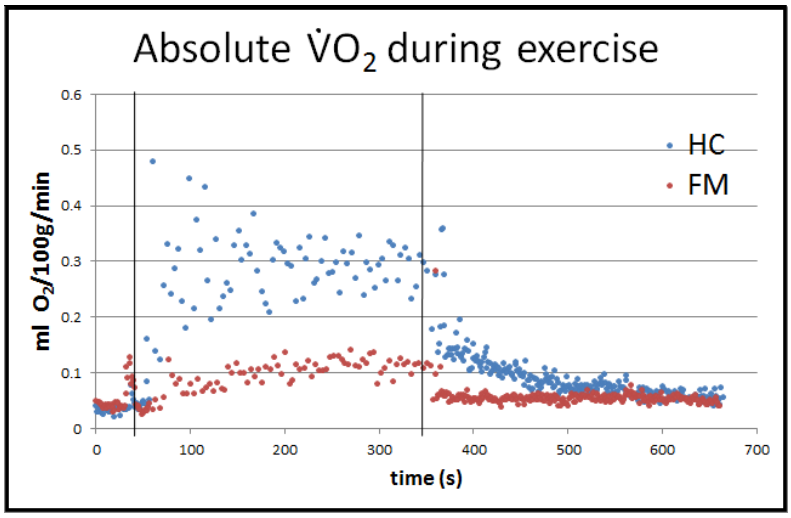

Figure 20. Individual HC and FM $\dot{V}O_2$ Response to Exercise

Raw absolute $\dot{V}O_2$ data in response to exercise for both a single HC subject and FM subject are shown. Vertical lines indicate the beginning and end of exercise. Pre-exercise $\dot{V}O_2$ value was 0.03 ml O_2/100 g/min for the HC subject and 0.04 ml O_2/100 g/min for the FM subject. Plateau $\dot{V}O_2$ values were 0.30 and 0.12 ml O_2/100 g/min for the HC and FM subjects, respectively.

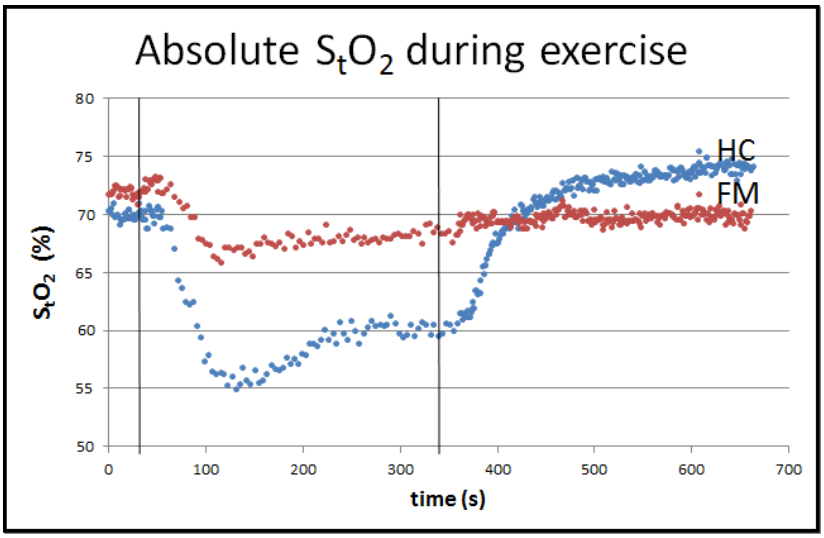

Figure 21. Individual HC and FM S_tO_2 Response to Exercise

Raw S_tO_2 data in response to exercise for both a single HC subject and FM subject are shown. Vertical lines indicate the beginning and end of exercise. Pre-exercise S_tO_2 value was 70.1% for the HC subject and 72.3% for the FM subject. Plateau S_tO_2 values were 59.9 and 68.7% for the HC and FM subjects, respectively.

5.4 Average Population Response

Subject data from both demographics demonstrated similar trends during occlusion and exercise. For all data, one FM subject's BF, S_tO_2, and $\dot{V}O_2$ data were not used following the 380 s time point, due to signal contamination from excessive movement by the subject that may have dislodged the optical probe. To observe the response to exercise more clearly, filtered BF, $\dot{V}O_2$, and S_tO_2 signals were averaged across the subject population at 10s time intervals throughout the protocol. The averaged exercise data are shown in Figures 22, 23, and 24. Results concerning the average baseline, pre-exercise, and plateau BF, $\dot{V}O_2$, and S_tO_2 values are summarized in Table 2.

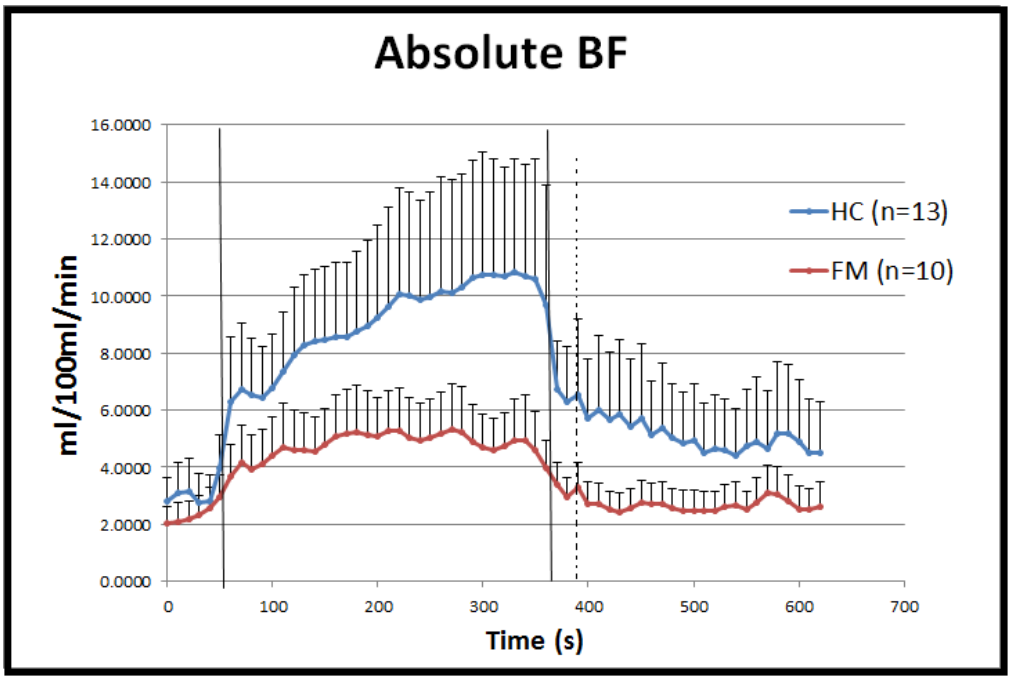

Figure 22. Average HC and FM Population BF Response to Exercise

The average absolute BF response to exercise of 10 subjects with fibromyalgia (FM) and 13 age-matched healthy controls (HC). For clarity, data were filtered and averaged at 10 s time intervals. The vertical lines indicate the beginning and end of exercise. Average pre-exercise BF value, determined as the average of data points 30 s before the onset of exercise, was 3.19 ± 1.03 ml/100 ml/min for the HC subjects and 2.63 ± 0.71 ml/100 ml/min for the FM subjects ($p = 0.444$). Plateau BF values were determined as the average of data points 30 s before the end of exercise. Plateau BF value, determined as the average of points 30 s before the end of exercise was 10.71 ± 3.91 ml/100 ml/min for HC subjects and 4.83 ± 1.42 ml/100 ml/min for FM subjects ($p = 0.018$). Note that at the dashed line, one FM subject's data were no longer used for averaging, due to signal contamination.

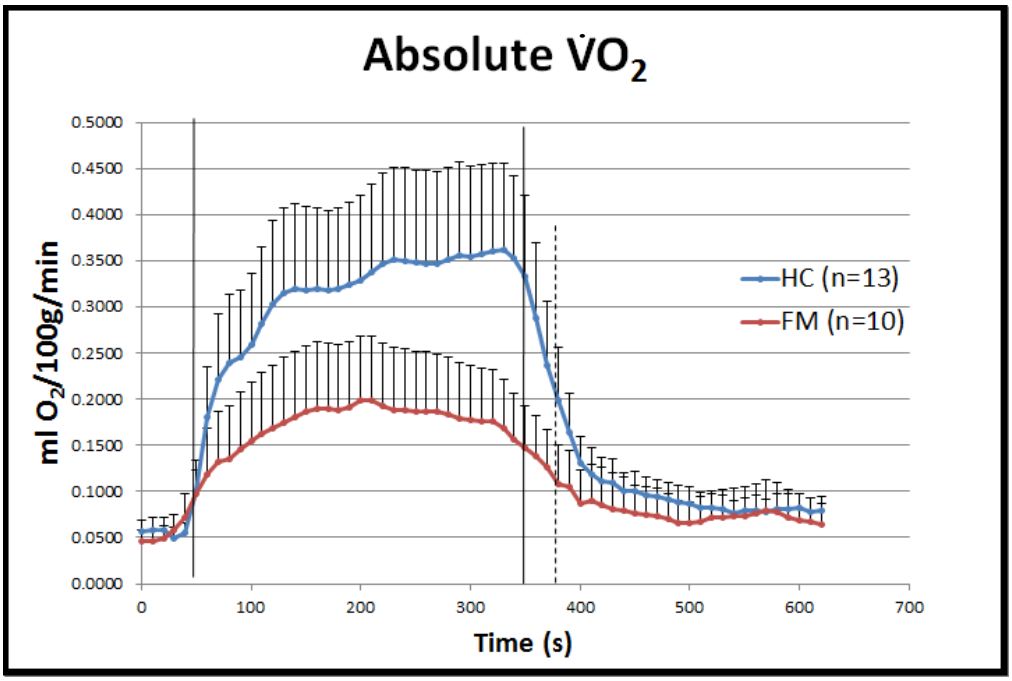

Figure 23. Average HC and FM Population $\dot{V}O_2$ Response to Exercise

The average absolute $\dot{V}O_2$ response to exercise of 10 subjects with fibromyalgia (FM) and 13 age-matched healthy controls (HC). For clarity, data were filtered and averaged at 10 s time intervals. The vertical lines indicate the beginning and end of exercise. Average pre-exercise $\dot{V}O_2$ value, determined as the average of data points 30 s before the onset of exercise, was 0.07 ± 0.02 ml O_2/100 g/min for the HC subjects and 0.08 ± 0.03 ml O_2/100 ml/min for the FM subjects (p = 0.690). Plateau $\dot{V}O_2$ values were determined as the average of data points 30 s before the end of exercise. Plateau $\dot{V}O_2$ value, determined as the average of points 30 s before the end of exercise was 0.35 ± 0.09 ml O_2/100 g/min for HC subjects and 0.16 ± 0.05 ml O_2/100 g/min for FM subjects (p = 0.002). At the dashed line, one FM subject's data were no longer used for averaging, due to signal contamination.

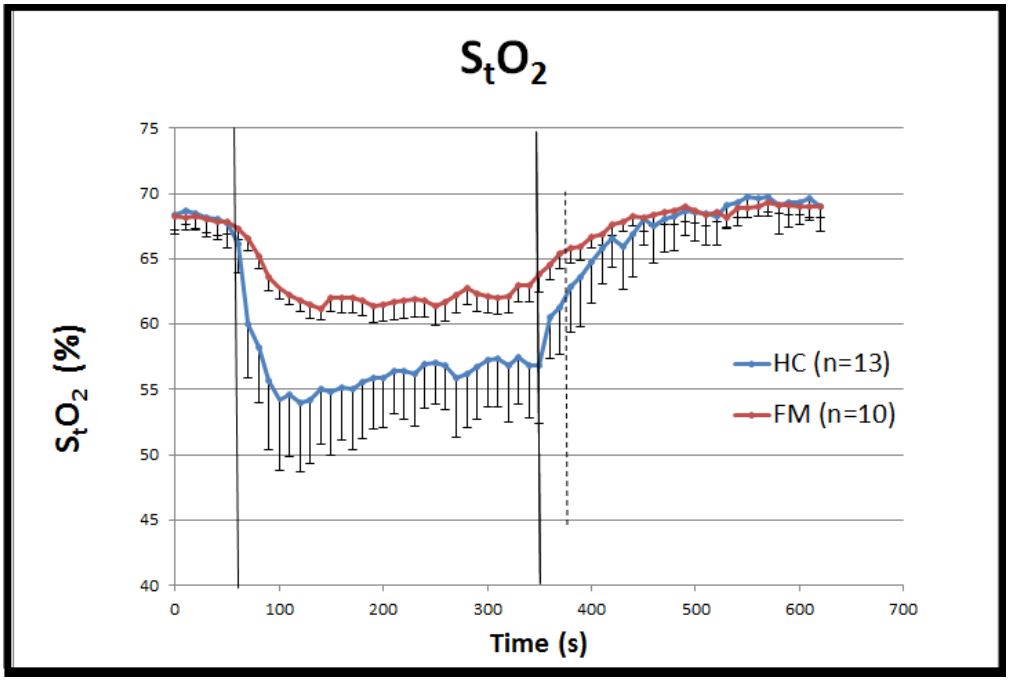

Figure 24. Average HC and FM Population S_tO_2 Response to Exercise

The average absolute S_tO_2 response to exercise of 10 subjects with fibromyalgia (FM) and 13 age-matched healthy controls (HC). For clarity, data were filtered and averaged at 10 s time intervals. The vertical lines indicate the beginning and end of exercise. Average pre-exercise S_tO_2 value, determined as the average of data points 30 s before the onset of exercise, was 68.0 ± 1.6% for the HC subjects and 67.9 ± 0.93% for the FM subjects ($p = 0.947$). Plateau S_tO_2 values were determined as the average of data points 30 s before the end of exercise. Plateau S_tO_2 value, determined as the average of points 30 s before the end of exercise was 57.1 ± 3.9% for HC subjects and 63.3 ± 1.3% for FM subjects ($p = 0.013$). Note that at the dashed line, one FM subject's data were no longer used for averaging, due to signal contamination.

Table 2. Exercise BF, $\dot{V}O_2$, and S_tO_2 Results for HC and FM Populations

Parameter	HC (n = 13)	FM (n = 10)	p-value (Student's t-test)
Baseline BF (ml/100 ml/min)	2.27 ± 0.52	2.42 ± 0.76	0.876
Baseline $\dot{V}O_2$ (ml O_2/100 g/min)	0.16 ± 0.05	0.10 ± 0.04	0.346
Baseline S_tO_2 (%)	69.1 ± 1.0	69.2 ± 0.9	0.920
Pre-exercise BF (ml/100 ml/min)	3.19 ± 1.03	2.63 ± 0.71	0.444
Pre-exercise $\dot{V}O_2$ (ml O_2/100 g/min)	0.07 ± 0.02	0.08 ± 0.03	0.690
Pre-exercise S_tO_2 (%)	68.0 ± 1.6	67.9 ± 0.93	0.947
Plateau BF (ml/100 ml/min)	10.71 ± 3.91	4.83 ± 1.42	0.018*
Plateau $\dot{V}O_2$ (ml O_2/100 g/min)	0.35 ± 0.09	0.16 ± 0.05	0.002*
Plateau S_tO_2 (%)	57.1 ± 3.9	63.3 ± 1.3	0.013*

CHAPTER 6: DISCUSSION AND CONCLUSIONS

This chapter begins with a discussion of the results from the two studies: the validation of the protocol in young healthy subjects (Chapter 6.1), and the application of the technique to a fibromyalgia population (Chapter 6.2). A comparison of baseline BF, V̇O2, StO2, and MVC between young and older healthy populations is given in Chapter 6.3. Next potential sources of error and challenges to the measurement technique are discussed in Chapter 6.4, including the influence of myoglobin on the optical signal, the influence of skin and adipose tissue, and the error introduced by assuming constant volume distribution, γ. The advantages and disadvantages of NIRS/DCS measurement compared to alternate modalities are reviewed in Chapter 6.5, and ideas for improvement of the gating algorithm are introduced in Chapter 6.6. Finally, a summary of conclusions regarding the reliability and applicability of the technique is given in Chapter 6.7.

6.1 Validation Results from Young Healthy Subjects Compared to Literature

The feasibility of this technique for monitoring absolute hemodynamic and metabolic responses in exercising muscle was assessed by comparison to results found in the literature using a variety of measurement techniques. For validation of plateau values towards the end of exercise, studies were investigated that employed dynamic forearm exercise within the same intensity range as the protocol described in Chapter 3. Comparisons for BF and $\dot{V}O_2$ are presented in Table 3. Because the literature studies with similar exercise protocol and intensity do not generally report S_tO_2 data, only the BF and $\dot{V}O_2$ data are used for comparison. As S_tO_2 is a part of the derived $\dot{V}O_2$

measurement, $\dot{V}O_2$ validation serves to corroborate S_tO_2 results. In addition, NIRS measurements of S_tO_2 have been previously validated with other techniques by many groups, including O_2 electrodes [96], ^{133}Xenon clearance [97], and indocyanine green [98-100].

The baseline BF and $\dot{V}O_2$ results were consistent with previously reported baseline values of BF [1, 8, 28, 29, 53, 54, 70, 76] and $\dot{V}O_2$ [1, 8, 28, 29, 53, 70, 76], as are the plateau values [1, 8, 76]. The dynamic physiological profiles of BF and $\dot{V}O_2$ changes during exercise also agree with the general profiles found in previous exercise studies [68, 101, 102]. One disagreement between these response profiles and the results presented in this study is the elevated BF/$\dot{V}O_2$ value during the recovery period following exercise, relative to the resting baseline value prior to exercise (see Figures 16, 17, and 18). While the origin of this shift has not yet been specifically identified, it is possible that it may be due to increased temperature at the probe site due to accumulated heat from exercising muscle trapped by the adhesive tape, which may increase Brownian motion and flow. Recent preliminary studies investigating the use of thinner adhesives such as Tegaderm®, as well as more open probe designs allowing for greater radiation of heat through the skin surface suggest that the shift may be mitigated by such intervention. Alternatively, it is possible that the light pressure from probe contact may induce a gradual hyperemic response [103, 104]. The shift may also be due to flow response differences between the microvasculature and large vessels measured by different modalities (e.g. DCS versus Doppler ultrasound) in different studies. Further investigation is necessary to verify the cause.

Table 3. Comparison of Validation Study Results to Literature

Study	Methods for measuring BF, $\dot{V}O_2$	Resting BF (ml/100ml/ min)	Exercise BF (ml/100ml/ min)	Resting $\dot{V}O_2$ (ml O_2/ 100g/min)	Exercise $\dot{V}O_2$ (ml O_2/ 100g/min)
†**(Van Beekvelt 2001)[28]**	NIRS + VO, NIRS + AO (n = 26)	0.72 ± 0.32	n/a	0.11 ± 0.03	n/a
†**(DeBlasi 1994)[1]**	NIRS + VO (n = 11)	1.9 ± 0.8	8.2 ± 2.9	0.10 ± 0.03	0.54 ± 0.24
†**(Harel 2008)[53]**	NIRS + VO (n = 25)	2.55 ± 0.10	n/a	n/a	n/a
††**(Van Beekvelt 1999)[105]**	NIRS + VO, NIRS + AO (n = 27)	0.719 ± 0.063	n/a	0.106 ± 0.006	n/a
†**(Edwards 1993)[54]**	NIRS + O_2 inspiration (n = 6)	2.35 ± 1.11	n/a	n/a	n/a
††**(Zelis 1974)[77]**	Strain gauge VO, blood samples (n = 22)	3.10 ± 0.27	7.10 ± 0.76	0.12 ± 0.01	0.51 ± 0.05
††**(Arnold 1990)[76]**	Strain gauge VO, blood samples (n = 8)	2.54 ± 0.23	9.20 ± 1.08	~0.1	~0.75
†**(Mottram 1955)[29]**	Strain gauge VO, blood samples (n = 16)	2.9 (0.09 – 0.52)	n/a	0.24 ± 0.07	n/a
††**(Gurley 2012 – present study)**	NIRS/DCS + VO, NIRS/DCS + AO (n = 9)	1.76 ± 0.42	8.93 ± 2.81	0.11 ± 0.03	0.57 ± 0.13

†Study results are represented as (mean ± SD). ††Study results are represented as (mean ± SE). Results presented without ranges are inferred from figures (i.e., values were not specifically stated in text). Measurements are on forearm flexor muscles of healthy adults. Studies including exercise data are for protocols which involve light/moderate rhythmic exercise at a similar intensity to that presented in the present study. Venous and arterial occlusion methods are represented as VO and AO, respectively. 'n/a', not applicable.

6.2 Results from Fibromyalgia Study

Tissue blood flow, oxygenation, and metabolism have all been previously investigated in fibromyalgia populations by means of Doppler ultrasound [5], laser Doppler [86, 90], biopsy [85, 89, 91, 92], dynamic fluorescence videomicroscopy [87], laser fluxmetry [88], O_2 electrodes [93], and ^{31}P-MRS [95]. Findings are controversial, and no study has investigated all three parameters (i.e., BF, $\dot{V}O_2$, and S_tO_2) simultaneously, noninvasively, and continuously during exercise. The present study investigated the feasibility of using a novel hybrid optical instrument and calibration protocol to investigate such parameters in FM and age-matched HC subjects during exercise. The results indicate that the applied technology has the potential to differentiate group differences and may fill a void in fibromyalgia research that other technologies cannot.

All subjects' data displayed similar trends in response to handgrip exercise. BF and $\dot{V}O_2$ increased in response to metabolic demand induced by exercise, and S_tO_2 correspondingly decreased as more oxygen was consumed from the tissue. In the study, no significant difference was found between HC and FM populations in BF, $\dot{V}O_2$, and S_tO_2 when comparing data points from 30 s of resting baseline data before exercise, but a significant difference was evident in all three variables from the last 30 s of exercise (see Section 5.4). In addition, the physiological profiles (see Figures 22, 23, and 24) qualitatively suggest a significant difference in BF, $\dot{V}O_2$, and S_tO_2 response to 50% MVC exercise between the two groups. Variables recover quickly following the end of exercise, suggesting that it may be difficult to observe differences between populations by only monitoring post-exercise data [5], further emphasizing the importance of quantifying muscle hemodynamic and metabolic responses *during* exercise.

The significant difference in plateau BF between HC and FM populations evident in the study results shows that FM subjects do not reach peak flows as high as HC subjects in response to the same fractional MVC exercise. The lower $\dot{V}O_2$ increase and lower S_tO_2 decrease in FM subjects during exercise indicate that there may also be some deficiency in oxygen utilization, which may be associated with poor mitochondrial function [106].

While the data presented shows that there is lower increase in BF and $\dot{V}O_2$, and lower decrease in S_tO_2 in FM subjects in response to exercise, it should be noted that there is a significant difference in the initial MVC between the groups. Consequently, the two groups had differing energy outputs during the exercise period. A lower work output naturally corresponds to a lower energy demand and $\dot{V}O_2$, which additionally translates to a lower flow requirement for the working muscle [107]. The difference in MVC may be attributed to deconditioning due to inactivity or the disease state itself. Although the FM subjects in this study were fairly fit, and had relatively comparable activity levels to the HC subjects, specific activities were not evaluated. For example, it is possible that the forearm muscle groups were less utilized than muscles of the leg during subjects' normal exercise routine, and were therefore more subject to deconditioning. It is also possible that subjects' gave varying levels of effort within the population. To ensure each subject was contracting at maximal voluntary effort, an interpolated twitch technique may be used in future [108]. There was no observed correlation between MVC and maximal BF, $\dot{V}O_2$, or S_tO_2. However, the extent to which this difference in MVC impacts the significance of the difference observed in the outcome variables has not yet been clarified, and requires further rigorous statistical analysis. To fully understand the

differences between HC and FM exercise response, groups of subjects with similar MVC should be tested to eliminate the effect of deconditioning that is commonly seen in FM patients [109]. In addition, larger groups of subjects should be recruited to ensure the significance of population differences and reduce the magnitude of the error bars in Figures 22, 23, and 24.

6.3 Comparison of Young and Older Healthy Subjects

A comparison of the baseline measurements from BF, $\dot{V}O_2$, and S_tO_2 in both the young and older healthy controls (Table 4) shows that values were very similar between healthy populations. This is in line with the findings of previous studies investigating hemodynamics/metabolism in response to aging [110, 111]. MVC was slightly, though not significantly lower in older HC, while the other parameters showed no significant differences. The plateau values cannot be reasonably compared between old and young healthy subjects due to the differing intensity exercise protocols (50% MVC versus 25% MVC), and are thus excluded from this comparison. In future studies, it may be interesting to investigate both young and older subject populations using the same exercise protocol to determine group differences. Larger subject populations may be able to more clearly define whether aging itself has an effect on muscle hemodynamics and metabolism.

Table 4. Comparison between Young and Older Healthy Subjects

Baseline Parameters	Young HC (n = 9)	Older HC (n = 13)	p-value (Student's t-test)
BF (ml/100 ml/min)	1.76 ± 0.4	2.27 ± 0.52	0.448
$\dot{V}O_2$ (ml O_2/100 g/min)	0.12 ± 0.02	0.16 ± 0.05	0.518
S_tO_2 (%)	68.0 ± 1.0	69.1 ± 1.0	0.464
MVC (N·m)	27.3 ± 0.6	24.14 ± 0.84	0.189

6.4 Study Limitations

Influence of Myoglobin on Oxygenation Measurements

In optical measurements of muscle tissue, there is some expected contamination of the signal due to the presence of cellular myoglobins, which have very similar optical spectra as hemoglobins [33]. Because of this overlap, the presence of both chromophores cannot be readily separated by NIR optical measurements. Many authors have argued the importance of this contamination, and most agree that NIR signals originate primarily (> 90%) from hemoglobins [33, 112, 113].

The technique developed in this study focuses on muscle oxygen consumption under moderate working conditions. Myoglobins have a much higher affinity for oxygen than hemoglobins [114], and for the mild physiological manipulations presented in this work, it is expected that myoglobins would remain mostly oxygenated. Therefore, dynamic oxygenation changes presented in these results may be viewed as a combined hemoglobin and myoglobin deoxygenation, with a minimal contribution from myoglobins. Furthermore, it is reasonable to expect that flow measurements (DCS) are not affected by myoglobin contamination, as myoglobins reside statically in the muscle tissues.

Detectable flow changes, by contrast, are determined from the moving red blood cells within the vasculature.

Influence of Adipose Tissue Thickness and Skin Blood Flow

One challenge facing NIR optical measurements is the influence of adipose tissue thickness (ATT), particularly in subjects with a higher BMI than average. The penetration depth of near-infrared light in biological tissue is roughly half that of the source-detector separation [28]. Although fat has low absorption in the NIR range [1], if the ATT layer is sufficiently thick, a larger portion of the detected signal could potentially originate from the skin and fat, and may therefore distort the true hemodynamic measurement of muscle. The measurements acquired in this study utilized a source-detector separation of 2.0 cm, which correlates to a probing depth of ~1 cm. The average ATT for the young healthy subject population was 1.5 ± 0.2 mm, and 3.1 ± 0.4 and 2.9 ± 0.4 for the FM and HC populations, respectively. This ATT is considerably less than this penetration depth, suggesting that the NIR light adequately probes muscle tissue. Previous work has shown that for a source-detector separation of 2 cm or greater, the contribution of the skin is < 5% of total light absorption, and the detected signal is mainly from muscle tissue [115]. Some researchers in the field have attempted to correct for light absorption in superficial tissues by using a two-layer model [33, 116]. Others have developed algorithms derived from Monte Carlo simulations with *in vivo* measurements [117] aimed at correcting for variation in measurement sensitivity due to ATT. These algorithms may be useful to employ in future work, especially where the subject population has highly varied ATT, or when investigating deeper muscle tissue.

The results of Niwayama's study [115] imply, however, that up to the ATT observed in this study (~3 mm), NIRS/DCS signal sensitivity is affected by less than 10%. In addition, no significant correlation between ATT and $\dot{V}O_2$ or BF was observed for any population. It is therefore reasonable to assume that skin and ATT did not adversely influence the measurements.

Influence of γ Assumption

In the derived calculation of $\dot{V}O_2$ (see Section 2.4), the percentage of blood contained in the venous compartment (γ) was assumed constant. However, there is a detectable change in blood volume during exercise, which manifests as an increase in [tHb] (average ~20% in the young healthy population). Because absorption is high in larger vessels, NIRS/DCS signals originate primarily from the arterioles, capillaries, and venules of the microvasculature [26]. It may be therefore assumed that the detected blood volume increase is due to changes in these small vessels.

Part of the observed volume increase is likely due to capillary recruitment, a normal physiological event which increases the area for metabolic exchange within muscle in response to increased demand from exercise [118]. Previous work in mathematical modeling of NIRS measurements [119] suggests that changes in blood volume during exercise are primarily due to the changes in number of microvascular units perfused, and attributes the volume increase to capillaries. In this case, capillary volume increase is neither in the arterial nor the venous compartment, and would have minimal effect on γ.

Part of the volume increase may also be due to changes in the venous compartment during exercise. Venules are considerably more compliant than arterioles, which makes

them more capable of accommodating volume changes. To evaluate the maximum impact this change could have on γ, assume the most dramatic case where the change in volume (Δ[tHb]) is due solely to changes in the venous compartment (V_v), while the volume in the arterial compartment remains constant (V_a). In this case an average ~20% Δ[tHb] (now indicative of ΔV_v) would cause a γ increase (where $\gamma = V_v/(V_v+V_a)$, see Section 2.4) from $\gamma_{rest} \approx 67\%$ [13] to $\gamma_{exercise} \approx 73\%$. This γ increase relates to a variation in $r\dot{V}O_2$ by a factor of ~7% $[(\gamma_{rest}/\gamma_{exercise} - 1) \times 100]$. Considering the fact that $r\dot{V}O_2$ increases several fold during exercise (see Figure 17), the minor variation introduced by assumption of constant γ may be considered unimportant. It should also be noted that variations in γ would only impact $\dot{V}O_2$ measurement, as BF is measured directly by the DCS without assuming any γ.

6.5 Advantages and Disadvantages of NIRS/DCS

The NIRS/DCS protocol developed in this study holds great promise for investigation of local hemodynamics and metabolism in muscle during exercise. However, one should consider the disadvantages as well as the benefits compared to alternative measurement techniques.

The primary advantage of NIRS/DCS technology is that it is entirely noninvasive, making the technique ideal for research purposes, especially with fragile patient populations, or pediatrics. Compared to catheterization or blood sampling [29] for $\dot{V}O_2$ measurement, NIRS/DCS requires much less setup and training, and is significantly more comfortable for the subject. The instrumentation of NIRS/DCS technology is also quite portable, which makes it an ideal diagnostic tool for subjects with limited mobility.

The running cost of a NIRS/DCS hybrid instrument is very inexpensive compared to other techniques which evaluate local perfusion and oxygen consumption [15]. PET, perfusion MRI, and ^{31}P-MRS all require significant initial investment, and consecutive measurements are expensive and require well-trained technicians. NIRS/DCS can easily be used for repeated measurements at very minimal cost. This is particularly beneficial in a research environment, where trial and error is an integral and unavoidable part of many studies.

This protocol also has the advantage of allowing continuous measurement during exercise. Many previous efforts using optical technology to evaluate hemodynamic and metabolic response to exercise have focused on monitoring values before and following exercise, due to the scattering effects of muscle motion [50], or the temporal limitations of measuring BF or $\dot{V}O_2$ via occlusion. It has been shown, however, that these dynamic parameters rapidly return to baseline following the end of exercise, or even exhibit hyperemic response in the case of heavy exercise [68]. Without continuous monitoring during and immediately following exercise, physiologically useful information may be lost between measurements.

NIRS/DCS is limited to measuring local perfusion under the probe site in the microvasculature. In some cases, measuring local flow can be preferable to monitoring limb flow, as muscle groups in the limbs can exhibit a great deal of heterogeneity in hemodynamic/metabolic response with aging or disease [17]. However, if a specific application requires quantification of regional or limb flow, measurement must be performed by monitoring the larger vessels. In this case, Doppler ultrasound is a popular method for measuring flow through major arteries. While this method is also

noninvasive and portable, it requires precise probe placement in relation to the vessel, which can become easily dislodged during exercise. To acquire muscle $\dot{V}O_2$ measurement in conjunction with Doppler ultrasound by the Fick method, additional blood sampling is required. These regional measurements are also not necessarily reflective of actual delivery and utilization of oxygen in local skeletal muscle [31].

Another restriction to the application of NIRS/DCS technology during exercise is that measurement is limited to only the relaxation phase of rhythmic exercise. By contrast, ultrasound Doppler can monitor flow throughout the entire contraction/relaxation cycle [15]. Flow is much higher in major arteries during relaxation compared to contraction [120], and it has been shown that arterial inflow occurs almost exclusively between contractions [121]. During contraction, microvascular perfusion is inhibited in part because of increased intramuscular pressure and extravascular compression [50]. Because NIRS/DCS monitors only the microvasculature, it is reasonable to confine BF and $\dot{V}O_2$ to the relaxation phase when using this measurement technique.

6.6 Future Improvements for Gating Algorithm

The gating algorithm developed for this study relies on the availability of a control signal from a dynamometer. In some cases, a dynamometer may not be readily available, or accessible, particularly for patients with limited mobility. In addition, the position of the dynamometer lever is a secondary measurement of muscle contraction. A more direct measure of muscle contraction status, such as EMG, would allow for more precise timing of data acquisition. Additionally, automatic initiation of the algorithm would be an effective solution to reduce the noise seen at the onset of exercise (see Figures 13, 14, and

15). Ideally, in future development of this protocol, EMG will be incorporated into the instrumentation as an alternative method to dynamometer-based signal control, and the gating algorithm will be fully automated.

6.7 Conclusions

This study demonstrates the novel application of NIRS and DCS technologies to continuously monitor absolute local muscle hemodynamic and metabolic parameters during exercise in a young healthy population, an older FM subject population, and an older age-matched healthy population. Previous problems with motion artifact during exercise were addressed with the use of an embedded software gating algorithm which monitored the muscle contraction status to determine appropriate times for data acquisition.

The results of the validation study in a young healthy population were consistent with previous literature findings, and the results of the fibromyalgia study showed significant differences in all three parameters of BF, $\dot{V}O_2$, and S_tO_2 at the end of moderate exercise. Although the results of this study are encouraging, further experimentation is required to fully validate the technique. The protocol has only been used with mild intensity exercise, and validation is of a qualitative nature (literature comparison). To fully establish the reliability of the technique, a range of exercise intensities and durations should be investigated, with concurrent measurement by another established modality (e.g. ASL-MRI, ^{31}P-MRS). Concurrent measurement would allow for quantitative multi-point comparison with thorough statistical analysis. A larger subject population would be desirable to reduce the perceived error due to normal physiological variation.

The results from the FM study indicate that the technology and protocol are suitable for monitoring hemodynamic and metabolic parameters in an older disease population, and can distinctly identify group differences. While the results of the study are inconclusive related to the pathophysiology underlying FM, due to the confounding variable of MVC, the study shows that the technique may be highly applicable to future investigations involving exercise response of patients diagnosed with FM. To further verify differences between the disease population and their healthy counterpart, a more carefully selected contingent of subjects with similar physical characteristics should be assessed. Larger groups may also help verify the validity of the observed differences, and reduce natural inter-subject variation.

Because muscle function is closely linked to oxidative metabolism and flow regulation, this technique is highly relevant for investigation of muscle physiology and pathology. The technique finds broad application to medical research, exercise physiology, sports medicine, disease diagnosis, and treatment evaluation. As spectroscopic technologies improve, this technique will become more accessible, with higher quality real-time data. The advantages suggest that NIRS/DCS would be an attractive alternative for more expensive or invasive methods of BF, S_tO_2, and $\dot{V}O_2$ quantification.

CHAPTER 7: SUMMARY AND PERSPECTIVES

In summary of this research study, I have presented a novel method for quantifying absolute muscle BF, tissue blood oxygenation, and $\dot{V}O_2$ simultaneously during rhythmic exercise, and demonstrated the potential application of the technique to investigating pathophysiology of disease which affects skeletal muscle. The method relies on a hybrid NIRS/DCS instrument for measurement, which was developed and built in our lab. Several facets of the design and completion of this study included my own contributions. These include design, construction, and integration of DCS photodetector power supply electronics (Chapter 2.3), design of the relative signal calibration protocol (Chapter 3.3), design of the exercise protocol (Chapter 3.4), co-development of the gating algorithm (Chapter 3.5), subject recruitment and acquisition of data in both a young healthy population, as well as FM subjects with age-matched HC subjects (Chapters 4 and 5), and general methods of data analysis (Chapters 4 and 5). The results of the validation study in young healthy subjects have also been peer-reviewed and published [122].

To appropriately evaluate skeletal muscle's regulatory ability, the oxygen demand (or oxygen consumption, $\dot{V}O_2$), the oxygen supply (BF), and the oxygen balance (S_tO_2) should all be evaluated simultaneously. Furthermore, it is critical to monitor the dynamic profiles of these variables in response to stimulus, as resting baseline values can obscure abnormalities, and the transient responses recover quickly. While NIRS and DCS have been able to provide a great deal of hemodynamic data individually, both must be used in order to evaluate $\dot{V}O_2$. The hybrid instrument developed in our lab combines the two spectroscopies in one streamlined measurement, providing a wealth of information that

gives a more complete picture of the local oxygenation kinetics within skeletal muscle than traditional methods.

This study has effectively addressed previous problems associated with DCS-based measurements, including quantification of relative signals and removal of motion artifact from skeletal muscle contraction. While the occlusion techniques used in the protocol to determine absolute baseline BF and $\dot{V}O_2$ are not new, the application to calibration of the direct but relative measurement during exercise has never been investigated, to the author's knowledge, and simultaneous absolute quantification of all presented parameters (BF, $\dot{V}O_2$, and S_tO_2) has never been achieved during exercise.

Another novel component of this study is the application of a dynamometer-based software gating algorithm to reduce motion artifact. The current algorithm is highly effective, but future development may further improve signal characteristics. Alternative sources for input signal, as well as more automated initiation and termination need to be investigated.

This study also demonstrates the first efforts to apply noninvasive optical technology to monitoring hemodynamics and metabolism continuously during exercise in fibromyalgia. While the results are somewhat inconclusive, the study shows the potential for using such technology to investigate responses to such stimulus in a fragile patient population, and could serve as a starting point for many other investigational studies on vasoregulation and metabolism in fibromyalgia. Data analysis for this study was achieved using custom MATLAB scripts, which read files generated by the hybrid instrument (see Chapter 2.3), and calculated continuous BF, $\dot{V}O_2$, and oxygenation variables (e.g. StO_2, [HbO_2], [Hb], [tHb]) (see Chapter 4).

The applications of this technique are many and varied. Normal muscle and exercise physiology, disease pathophysiology, diagnosis, treatment evaluation, sports medicine and rehabilitation all benefit from the ability to continuously monitor local hemodynamic and metabolic regulation. The method and instrument are especially suited to a research and clinical environment, due to the noninvasive, inexpensive, and portable nature of the technology. The findings of this study further push the limits of optical measurement in medicine.

APPENDIX A: GLOSSARY

SYMBOLS

α	Ratio of Dynamic to Static Scatterers (0-1)
ac	Modulated Light Amplitude
C	Hemoglobin Concentration of Whole Blood
γ	Percentage of Blood Volume Contained in the Venous Compartment
D	Photon Diffusion Constant
D_B	Effective Diffusion Coefficient
dc	Average Light Intensity
g_1	Normalized Electric Field Temporal Autocorrelation Function
G_1	Unnormalized Electric Field Temporal Autocorrelation Function
g_2	Normalized Intensity Temporal Autocorrelation Function
I	Intensity
k_0	Wavevector of Photons in Medium ($k_0 = 2\pi n/\lambda$)
λ	Wavelength
n	Ratio of Sample and Air Index of Refraction
φ	Phase Modulation of NIR Light
r	Source-detector Separation
r	Position Vector
ρ	Source-detector Separation
$\langle \Delta r^2(\tau) \rangle$	Mean-square Displacement of Scatterers during τ
S_{ac}	Slope of r vs. $\ln(ac \cdot r^2)$ Curve
S_{dc}	Slope of r vs. $\ln(dc \cdot r^2)$ Curve

S_φ	Slope of r vs.φ Curve
S_0	Source-light Distribution
τ	Correlation Function Decay Time
μ_a	Absorption Coefficient
μ_s'	Reduced Scattering Coefficient
[x]	Concentration of x
v	Speed of Light in Medium
V_a	Blood Volume in the Arterial Compartment
V_v	Blood Volume in the Venous Compartment
ω	Angular Frequency of Modulation

TERMS

APD	Avalanche Photodiode
ASL-MRI	Arterial Spin-Labeled Magnetic Resonance Imaging (Perfusion MRI)
ATT	Adipose Tissue Thickness
BF	Blood Flow
BFI	Blood Flow Index (αD_B)
CW	Continuous Wave
DCS	Diffuse Correlation Spectroscopy
DLS	Dynamic Light Scattering
DWS	Diffusing Wave Spectroscopy
FD	Frequency Domain
FM	Fibromyalgia

Hb	Deoxy-hemoglobin
HbO_2	Oxy-hemoglobin
HC	Healthy Control
MVC	Maximal Voluntary Contraction
NIR	Near-Infrared
NIRS	Near-Infrared Spectroscopy
$[O]_a$	Arterial Oxygen Concentration
$[O]_v$	Venous Oxygen Concentration
OEF	Oxygen Extraction Fraction
^{31}P-MRS	31-phosphorus Magnetic Resonance Spectroscopy
PET	Positron Emission Tomography
PMT	Photomultiplier Tube
RBC	Red Blood Cell
SNR	Signal to Noise Ratio
S_aO_2	Arterial Blood Oxygen Saturation
S_tO_2	Tissue Blood Oxygen Saturation
TD	Time Domain
tHb	Total Hemoglobin
$\dot{V}O_2$	Oxygen Consumption Rate

REFERENCES

1. De Blasi, R.A., Ferrari, M., Natali, A., Conti, G., Mega, A., and Gasparetto, A., *Noninvasive Measurement of Forearm Blood-Flow and Oxygen-Consumption by near-Infrared Spectroscopy.* Journal of Applied Physiology, 1994. **76**(3): p. 1388-1393.
2. Cheatle, T.R., Potter, L.A., Cope, M., Delpy, D.T., Smith, P.D.C., and Scurr, J.H., *Near-Infrared Spectroscopy in Peripheral Vascular-Disease.* British Journal of Surgery, 1991. **78**(4): p. 405-408.
3. Wolf, U., Wolf, M., Choi, J.H., Levi, M., Choudhury, D., Hull, S., Coussirat, D., Paunescu, L.A., Safonova, L.P., Michalos, A., Mantulin, W.W., and Gratton, E., *Localized irregularities in hemoglobin flow and oxygenation in calf muscle in patients with peripheral vascular disease detected with near-infrared spectrophotometry.* Journal of Vascular Surgery, 2003. **37**(5): p. 1017-1026.
4. Shammas, N.W., *Epidemiology, classification, and modifiable risk factors of peripheral arterial disease.* Vascular Health Risk Management, 2007. **3**(2): p. 229-234.
5. Elvin, A., Sioteen, A.K., Nilsson, A., and Kosek, E., *Decreased muscle blood flow in fibromyalgia patients during standardised muscle exercise: A contrast media enhanced colour doppler study.* European Journal of Pain, 2006. **10**(2): p. 137-144.
6. Mease, P., *Fibromyalgia syndrome: Review of clinical presentation, pathogenesis, outcome measures, and treatment.* Journal of Rheumatology, 2005. **32**: p. 6-21.
7. Arnold, J.M.O., Ribeiro, J.P., and Colucci, W.S., *Muscle Blood-Flow during Forearm Exercise in Patients with Severe Heart-Failure.* Circulation, 1990. **82**(2): p. 465-472.
8. Zelis, R., Longhurs.J, Capone, R.J., and Mason, D.T., *Comparison of Regional Blood-Flow and Oxygen Utilization during Dynamic Forearm Exercise in Normal Subjects and Patients with Congestive Heart-Failure.* Circulation, 1974. **50**(1): p. 137-143.
9. Croft, J.B., Giles, W.H., Pollard, R.A., Keenan, N.L., Casper, M.L., and Anda, R.F., *Heart failure survival among older adults in the United States: a poor prognosis for an emerging epidemic in the Medicare population.* Archives of Internal Medicine, 1999. **159**(5): p. 505-510.
10. Hamaoka, T., McCully, K.K., Niwayama, M., and Chance, B., *The use of muscle near-infrared spectroscopy in sport, health and medical sciences: recent developments.* Philosophical Transactions of the Royal Society a-Mathematical Physical and Engineering Sciences, 2011. **369**(1955): p. 4591-4604.
11. Jasperse, J.L., Seals, D.R., and Callister, R., *Active Forearm Blood-Flow Adjustments to Handgrip Exercise in Young and Older Healthy-Men.* Journal of Physiology-London, 1994. **474**(2): p. 353-360.
12. McCully, K.K., Halber, C., and Posner, J.D., *Exercise-Induced Changes in Oxygen-Saturation in the Calf Muscles of Elderly Subjects with Peripheral Vascular-Disease.* Journals of Gerontology, 1994. **49**(3): p. B128-B134.

13. Yu, G., Durduran, T., Lech, G., Zhou, C., Chance, B., Mohler, E.R., 3rd, and Yodh, A.G., *Time-dependent blood flow and oxygenation in human skeletal muscles measured with noninvasive near-infrared diffuse optical spectroscopies.* Journal of Biomedical Optics, 2005. **10**(2): p. 024027.
14. Feringa, H.H.H., Bax, J.J.J., van Waning, V.H., Boersma, E., Elhendy, A., Schouten, O., Tangelder, M.J., van Sambeek, M.H.R.M., van den Meiracker, A.H., and Poldermans, D., *The long-term prognostic value of the resting and postexercise ankle-brachial index.* Archives of Internal Medicine, 2006. **166**(5): p. 529-535.
15. Radegran, G., *Limb and skeletal muscle blood flow measurements at rest and during exercise in human subjects.* Proceedings of the Nutrition Society, 1999. **58**(4): p. 887-898.
16. Sehgal, C.M., Arger, P.H., Rowling, S.E., Conant, E.F., Reynolds, C., and Patton, J.A., *Quantitative vascularity of breast masses by Doppler imaging: Regional variations and diagnostic implications.* Journal of Ultrasound in Medicine, 2000. **19**(7): p. 427-440.
17. Musch, T.I., Eklund, K.E., Hageman, K.S., and Poole, D.C., *Altered regional blood flow responses to submaximal exercise in older rats.* Journal of Applied Physiology, 2004. **96**(1): p. 81-88.
18. Kalliokoski, K.K., Kemppainen, J., Larmola, K., Takala, T.O., Peltoniemi, P., Oksanen, A., Ruotsalainen, U., Cobelli, C., Knuuti, J., and Nuutila, P., *Muscle blood flow and flow heterogeneity during exercise studied with positron emission tomography in humans.* European Journal of Applied Physiology, 2000. **83**(4-5): p. 395-401.
19. Wahlberg, E., Olofsson, P., Swedenborg, J., and Fagrell, B., *Level of Arterial-Obstruction in Patients with Peripheral Arterial Occlusive Disease (Paod) Determined by Laser-Doppler Fluxmetry.* European Journal of Vascular Surgery, 1993. **7**(6): p. 684-689.
20. Baron, J.C., *Mapping the ischaemic penumbra with PET: Implications for acute stroke treatment.* Cerebrovascular Diseases, 1999. **9**(4): p. 193-201.
21. Schmitt, P., Kotas, M., Tobermann, A., Haase, A., and Flentje, M., *Quantitative tissue perfusion measurements in head and neck carcinoma patients before and during radiation therapy with a non-invasive MR imaging spin-labeling technique.* Radiotherapy and Oncology, 2003. **67**(1): p. 27-34.
22. Pilon, C.S., Leathley, M., London, R., McLean, S., Phang, P.T., Priestley, R., Rosenberg, F.M., Singer, J., Anis, A.H., and Dodek, P.M., *Practice guideline for arterial blood gas measurement in the intensive care unit decreases numbers and increases appropriateness of tests.* Critical Care Medicine, 1997. **25**(8): p. 1308-1313.
23. Haacke, E.M., Lai, S., Reichenbach, J.R., Kuppusamy, K., Hoogenraad, F.G., Takeichi, H., and Lin, W., *In vivo measurement of blood oxygen saturation using magnetic resonance imaging: a direct validation of the blood oxygen level-dependent concept in functional brain imaging.* Human Brain Mapping, 1997. **5**(5): p. 341-346.
24. Heineman, W.R. and Jensen, W.B., *Leland C. Clark Jr. (1918-2005).* Biosensors & Bioelectronics, 2006. **21**(8): p. 1403-1404.

25. Vanderkooi, J.M., Erecinska, M., and Silver, I.A., *Oxygen in Mammalian Tissue - Methods of Measurement and Affinities of Various Reactions.* American Journal of Physiology, 1991. **260**(6): p. C1131-C1150.
26. Boushel, R., Langberg, H., Olesen, J., Gonzales-Alonzo, J., Bulow, J., and Kjaer, M., *Monitoring tissue oxygen availability with near infrared spectroscopy (NIRS) in health and disease.* Scandinavian Journal of Medicine & Science in Sports, 2001. **11**(4): p. 213-222.
27. Smithies, M.N., Royston, B., Makita, K., Konieczko, K., and Nunn, J.F., *Comparison of Oxygen-Consumption Measurements - Indirect Calorimetry Versus the Reversed Fick Method.* Critical Care Medicine, 1991. **19**(11): p. 1401-1406.
28. Van Beekvelt, M.C., Colier, W.N.J.M., Wevers, R.A., and van Engelen, B.G.M., *Performance of near-infrared spectroscopy in measuring local O-2 consumption and blood flow in skeletal muscle.* Journal of Applied Physiology, 2001. **90**(2): p. 511-519.
29. Mottram, R.F., *The Oxygen Consumption of Human Skeletal Muscle Invivo.* Journal of Physiology-London, 1955. **128**(2): p. 268-276.
30. Sako, T., Hamaoka, T., Higuchi, H., Kurosawa, Y., and Katsumura, T., *Validity of NIR spectroscopy for quantitatively measuring muscle oxidative metabolic rate in exercise.* Journal of Applied Physiology, 2001. **90**(1): p. 338-344.
31. McCully, K.K. and Hamaoka, T., *Near-infrared spectroscopy: what can it tell us about oxygen saturation in skeletal muscle?* Exercise and Sport Sciences Review, 2000. **28**(3): p. 123-127.
32. Kuebler, W.M., *How NIR is the future in blood flow monitoring?* Journal of Applied Physiology, 2008. **104**(4): p. 905-906.
33. Durduran, T., *Non-invasive measurements of tissue hemodynamics with hybrid diffuse optical methods*, Ph.D. Dissertation, 2004, University of Pennsylvania.
34. Ferrari, M., Muthalib, M., and Quaresima, V., *The use of near-infrared spectroscopy in understanding skeletal muscle physiology: recent developments.* Philosophical Transactions of the Royal Society a-Mathematical Physical and Engineering Sciences, 2011. **369**(1955): p. 4577-4590.
35. Boas, D.A., Campbell, L.E., and Yodh, A.G., *Scattering and Imaging with Diffusing Temporal Field Correlations.* Physical Review Letters, 1995. **75**(9): p. 1855-1858.
36. Yu, G., Durduran, T., Zhou, C., Cheng, R., and Yodh, A., *Near-infrared Diffuse Correlation Spectroscopy (DCS) for Assessment of Tissue Blood Flow*, in *Handbook of Biomedical Optics*, D.A. Boas, C. Pitris, and N. Ramanujam, Editors. 2010, Taylor & Francis Books, Inc.
37. Shang, Y., Cheng, R., Dong, L., Ryan, S.J., Saha, S.P., and Yu, G., *Cerebral monitoring during carotid endarterectomy using near-infrared diffuse optical spectroscopies and electroencephalogram.* Physics in Medicine and Biology, 2011. **56**(10): p. 3015-3032.
38. Buckley, E., Cook, N., Durduran, T., Kim, M., Zhou, C., Choe, R., Yu, G., Licht, D., Detre, J., Greenberg, J., Hurt, H., and Yodh, A., *Cerebral hemodynamics of preterm infants during postural intervention measured with diffuse correlation*

spectroscopy and transcranial doppler ultrasound. Journal of Cerebral Blood Flow and Metabolism, 2009. **29**: p. S470-S471.
39. Kim, M.N., Durduran, T., Frangos, S., Edlow, B.L., Buckley, E.M., Moss, H.E., Zhou, C., Yu, G., Choe, R., Maloney-Wilensky, E., Wolf, R.L., Grady, M.S., Greenberg, J.H., Levine, J.M., Yodh, A.G., Detre, J.A., and Kofke, W.A., *Noninvasive measurement of cerebral blood flow and blood oxygenation using near-infrared and diffuse correlation spectroscopies in critically brain-injured adults.* Neurocritical Care, 2010. **12**(2): p. 173-180.
40. Zhou, C., *In-vivo optical imaging and spectroscopy of cerebral hemodynamics*, Ph.D., 2007, University of Pennsylvania.
41. Durduran, T., Yu, G., Burnett, M.G., Detre, J.A., Greenberg, J.H., Wang, J.J., Zhou, C., and Yodh, A.G., *Diffuse optical measurement of blood flow, blood oxygenation, and metabolism in a human brain during sensorimotor cortex activation.* Optics Letters, 2004. **29**(15): p. 1766-1768.
42. Cheng, R., Shang, Y., Hayes, D., Saha, S., and Yu, G., *Noninvasive optical evaluation of spontaneous low frequency oscillations in cerebral hemodynamics.* NeuroImage, 2012. **On-line**(http://dx.doi.org/10.1016/j.neuroimage.2012.05.069): p. (in press).
43. Sunar, U., Quon, H., Durduran, T., Zhang, J., Du, J., Zhou, C., Yu, G., Choe, R., Kilger, A., Lustig, R., Loevner, L., Nioka, S., Chance, B., and Yodh, A.G., *Noninvasive diffuse optical measurement of blood flow and blood oxygenation for monitoring radiation therapy in patients with head and neck tumors: a pilot study.* Journal of Biomedical Optics, 2006. **11**(6): p. 051903.
44. Dong, L.X., Kudrimoti, M., Cheng, R., Shang, Y., Johnson, E.L., Stevens, S.D., Shelton, B.J., and Yu, G., *Noninvasive diffuse optical monitoring of head and neck tumor blood flow and oxygenation during radiation delivery.* Biomedical Optics Express, 2012. **3**(2): p. 259-272.
45. Zhou, C., Choe, R., Shah, N., Durduran, T., Yu, G., Durkin, A., Hsiang, D., Mehta, R., Butler, J., Cerussi, A., Tromberg, B.J., and Yodh, A.G., *Diffuse optical monitoring of blood flow and oxygenation in human breast cancer during early stages of neoadjuvant chemotherapy.* Journal of Biomedical Optics, 2007. **12**(5): p. 051903.
46. Durduran, T., Choe, R., Yu, G., Zhou, C., Tchou, J.C., Czerniecki, B.J., and Yodh, A.G., *Diffuse optical measurement of blood flow in breast tumors.* Optics Letters, 2005. **30**(21): p. 2915-2917.
47. Munk, N., Symons, B., Shang, Y., Cheng, R., and Yu, G., *Noninvasively measuring the hemodynamic effects of massage on skeletal muscle: A novel hybrid near-infrared diffuse optical instrument.* Journal of Bodywork and Movement Therapy, 2012. **16**(1): p. 22-28.
48. Yu, G., Shang, Y., Zhao, Y., Cheng, R., Dong, L., and Saha, S., *Intraoperative evaluation of revascularization effect on ischemic muscle hemodynamics using near-infrared diffuse optical spectroscopies.* Journal of Biomedical Optics, 2011. **16**(2): p. 027004.
49. Yu, G., Floyd, T.F., Durduran, T., Zhou, C., Wang, J., Detre, J.A., and Yodh, A.G., *Validation of diffuse correlation spectroscopy for muscle blood flow with*

concurrent arterial spin labeled perfusion MRI. Optics Express, 2007. **15**(3): p. 1064-1075.
50. Shang, Y., Symons, T.B., Durduran, T., Yodh, A.G., and Yu, G., *Effects of muscle fiber motion on diffuse correlation spectroscopy blood flow measurements during exercise.* Biomedical Optics Express, 2010. **1**(2): p. 500-511.
51. Belau, M., Ninck, M., Hering, G., Spinelli, L., Contini, D., Torricelli, A., and Gisler, T., *Noninvasive observation of skeletal muscle contraction using near-infrared time-resolved reflectance and diffusing-wave spectroscopy.* Journal of Biomedical Optics, 2010. **15**(5): p. 057007.
52. Hamaoka, T., Iwane, H., Shimomitsu, T., Katsumura, T., Murase, N., Nishio, S., Osada, T., Kurosawa, Y., and Chance, B., *Noninvasive measures of oxidative metabolism on working human muscles by near-infrared spectroscopy.* Journal of Applied Physiology, 1996. **81**(3): p. 1410-1417.
53. Harel, F., Denault, A., Ngo, Q., Dupuis, J., and Khairy, P., *Near-infrared spectroscopy to monitor peripheral blood flow perfusion.* Journal of Clinical Monitoring and Computing, 2008. **22**(1): p. 37-43.
54. Edwards, A.D., Richardson, C., van der Zee, P., Elwell, C., Wyatt, J.S., Cope, M., Delpy, D.T., and Reynolds, E.O., *Measurement of hemoglobin flow and blood flow by near-infrared spectroscopy.* Journal of Applied Physiology, 1993. **75**(4): p. 1884-1889.
55. De Blasi, R.A., Cope, M., Elwell, C., Safoue, F., and Ferrari, M., *Noninvasive Measurement of Human Forearm Oxygen-Consumption by near-Infrared Spectroscopy.* European Journal of Applied Physiology, 1993. **67**(1): p. 20-25.
56. Colier, W.N.J.M., Meeuwsen, I.B.A.E., Degens, H., and Oeseburg, B., *Determination of Oxygen-Consumption in Muscle during Exercise Using near-Infrared Spectroscopy.* Acta Anaesthesiologica Scandinavica, 1995. **39**: p. 151-155.
57. Fantini, S., Franceschini, M.A., and Gratton, E., *Semi-Infinite-Geometry Boundary-Problem for Light Migration in Highly Scattering Media - a Frequency-Domain Study in the Diffusion-Approximation.* Journal of the Optical Society of America B-Optical Physics, 1994. **11**(10): p. 2128-2138.
58. Shang, Y., Zhao, Y., Cheng, R., Dong, L., Irwin, D., and Yu, G., *Portable optical tissue flow oximeter based on diffuse correlation spectroscopy.* Optics Letters, 2009. **34**(22): p. 3556-3558.
59. Hueber, D., Fantini, S., Cerussi, A., and Barbieria, B., *New Optical Probe Designs for Absolute (Self-calibrating) NIR Tissue Hemoglobin Measurements.* SPIE Proceedings, 1999. **3597**: p. 618-631.
60. Wallace, D., Michener, B., Choudhury, D., Levi, M., Fennelly, P., Hueber, D., and Barbieri, B. *Summary of the results of a 95 subject human clinical trial for the diagnosis of peripheral vascular disease using a near infrared frequency domain hemoglobin spectrometer*. in *SPIE Conference on Optical Tomography and Spectroscopy of Tissue Ill*. 1999. San Jose, CA, USA: Society of Photo-Optical Instrumentation Engineers.
61. Fantini, S., Hueber, D., Franceschini, M.A., Gratton, E., Rosenfeld, W., Stubblefield, P.G., Maulik, D., and Stankovic, M.R., *Non-invasive optical*

monitoring of the newborn piglet brain using continuous-wave and frequency-domain spectroscopy. Phys Med Biol, 1999. **44**(6): p. 1543-1563.
62. Maret, G. and Wolf, P.E., *Multiple Light-Scattering from Disordered Media - the Effect of Brownian-Motion of Scatterers.* Zeitschrift Fur Physik B-Condensed Matter, 1987. **65**(4): p. 409-413.
63. Boas, D.A. and Yodh, A.G., *Spatially varying dynamical properties of turbid media probed with diffusing temporal light correlation.* Journal of the Optical Society of America a-Optics Image Science and Vision, 1997. **14**(1): p. 192-215.
64. Rice, S.O., *Mathematical Analysis of Random Noise.* Bell Systems Tech. J., 1944. **23**: p. 282-332.
65. Culver, J.P., Durduran, T., Furuya, T., Cheung, C., Greenberg, J.H., and Yodh, A.G., *Diffuse optical tomography of cerebral blood flow, oxygenation, and metabolism in rat during focal ischemia.* Journal of Cerebral Blood Flow and Metabolism, 2003. **23**(8): p. 911-924.
66. Mayhew, J., Johnston, D., Martindale, J., Jones, M., Berwick, J., and Zheng, Y., *Increased oxygen consumption following activation of brain: Theoretical footnotes using spectroscopic data from barrel cortex.* Neuroimage, 2001. **13**(6): p. 975-987.
67. Quaresima, V., Homma, S., Azuma, K., Shimizu, S., Chiarotti, F., Ferrari, M., and Kagaya, A., *Calf and shin muscle oxygenation patterns and femoral artery blood flow during dynamic plantar flexion exercise in humans.* European Journal of Applied Physiology, 2001. **84**(5): p. 387-394.
68. Van Beekvelt, M.C., Shoemaker, J.K., Tschakovsky, M.E., Hopman, M.T.E., and Hughson, R.L., *Blood flow and muscle oxygen uptake at the onset and end of moderate and heavy dynamic forearm exercise.* American Journal of Physiology-Regulatory Integrative and Comparative Physiology, 2001. **280**(6): p. R1741-R1747.
69. Wilkinson, I.B. and Webb, D.J., *Venous occlusion plethysmography in cardiovascular research: methodology and clinical applications.* British Journal of Clinical Pharmacology, 2001. **52**(6): p. 631-646.
70. Van Beekvelt, M.C., Colier, W.N., Wevers, R.A., and Van Engelen, B.G., *Quantitative measurement of oxygen consumption and forearm blood flow in patients with mitochondrial myopathies.* Advances in Experimental Medicine and Biology, 1999. **471**: p. 313-319.
71. Groothuis, J.T., van Vliet, L., Kooijman, M., and Hopman, M.T.E., *Venous cuff pressures from 30 mmHg to diastolic pressure are recommended to measure arterial inflow by plethysmography.* Journal of Applied Physiology, 2003. **95**(1): p. 342-347.
72. Paunescu, L., *Tissue blood flow and oxygen consumption measured with near-infrared frequency-domain spectroscopy*, in *Biophysics and Computational Biology*, Ph.D. Dissertation 2001, University of Illinois at Urbana-Champaign.
73. Van Straten, A.H., Hamad, M.A., van Zundert, A.J., Martens, E.J., Schonberger, J.P., and de Wolf, A.M., *Preoperative hemoglobin level as a predictor of survival after coronary artery bypass grafting: a comparison with the matched general population.* Circulation, 2009. **120**(2): p. 118-125.

74. Barker, S.J., Curry, J., Redford, D., and Morgan, S., *Measurement of carboxyhemoglobin and methemoglobin by pulse oximetry - A human volunteer study.* Anesthesiology, 2006. **105**(5): p. 892-897.
75. Billett, H.H., *Hemoglobin and Hematocrit*, in *Clinical Methods: The History, Physical, and Laboratory Examinations*, H.K. Walker, W.D. Hall, and J.W. Hurst, Editors. 1990, Butterworth Publishers: Boston.
76. Arnold, J.M., Ribeiro, J.P., and Colucci, W.S., *Muscle blood flow during forearm exercise in patients with severe heart failure.* Circulation, 1990. **82**(2): p. 465-472.
77. Zelis, R., Longhurst, J., Capone, R.J., and Mason, D.T., *A comparison of regional blood flow and oxygen utilization during dynamic forearm exercise in normal subjects and patients with congestive heart failure.* Circulation, 1974. **50**(1): p. 137-143.
78. Graham, W., *The fibrositis syndrome.* Treatment Services Bulletin, 1953. **8**(7): p. 400-404.
79. Wolfe, F., Smythe, H.A., Yunus, M.B., Bennett, R.M., Bombardier, C., Goldenberg, D.L., Tugwell, P., Campbell, S.M., Abeles, M., Clark, P., and et al., *The American College of Rheumatology 1990 Criteria for the Classification of Fibromyalgia. Report of the Multicenter Criteria Committee.* Arthritis and Rheumatism, 1990. **33**(2): p. 160-172.
80. Wolfe, F., Ross, K., Anderson, J., Russell, I.J., and Hebert, L., *The prevalence and characteristics of fibromyalgia in the general population.* Arthritis and Rheumatism, 1995. **38**(1): p. 19-28.
81. Abeles, A.M., Pillinger, M.H., Solitar, B.M., and Abeles, M., *Narrative review: The pathophysiology of fibromyalgia.* Annals of Internal Medicine, 2007. **146**(10): p. 726-734.
82. Mannerkorpi, K., *Exercise in fibromyalgia.* Current Opinions in Rheumatology, 2005. **17**(2): p. 190-194.
83. Yildiz, S., Kiralp, M.Z., Akin, A., Keskin, I., Ay, H., Dursun, H., and Cimsit, M., *A new treatment modality for fibromyalgia syndrome: hyperbaric oxygen therapy.* Journal of International Medical Research, 2004. **32**(3): p. 263-267.
84. Katz, D.L., Greene, L., Ali, A., and Faridi, Z., *The pain of fibromyalgia syndrome is due to muscle hypoperfusion induced by regional vasomotor dysregulation.* Medical Hypotheses, 2007. **69**(3): p. 517-525.
85. Larsson, S.E., Bengtsson, A., Bodegard, L., Henriksson, K.G., and Larsson, J., *Muscle Changes in Work-Related Chronic Myalgia.* Acta Orthopaedica Scandinavica, 1988. **59**(5): p. 552-556.
86. Larsson, S.E., Bodegard, L., Henriksson, K.G., and Oberg, P.A., *Chronic Trapezius Myalgia - Morphology and Blood-Flow Studied in 17 Patients.* Acta Orthopaedica Scandinavica, 1990. **61**(5): p. 394-398.
87. Grassi, W., Core, P., Carlino, G., Salaffi, F., and Cervini, C., *Capillary permeability in fibromyalgia.* Journal of Rheumatology, 1994. **21**(7): p. 1328-1331.
88. Morf, S., Amann-Vesti, B., Forster, A., Franzeck, U.K., Koppensteiner, R., Uebelhart, D., and Sprott, H., *Microcirculation abnormalities in patients with*

fibromyalgia - measured by capillary microscopy and laser fluxmetry. Arthritis Research & Therapy, 2005. **7**(1): p. R209-R216.
89. McIver, K.L., Evans, C., Kraus, R.M., Ispas, L., Sciotti, V.M., and Hickner, R.C., *NO-mediated alterations in skeletal muscle nutritive blood flow and lactate metabolism in fibromyalgia.* Pain, 2006. **120**(1-2): p. 161-169.
90. Jeschonneck, M., Grohmann, G., Hein, G., and Sprott, H., *Abnormal microcirculation and temperature in skin above tender points in patients with fibromyalgia.* Rheumatology, 2000. **39**(8): p. 917-921.
91. Bartels, E.M. and Danneskioldsamsoe, B., *Histological Abnormalities in Muscle from Patients with Certain Types of Fibrositis.* Lancet, 1986. **1**(8484): p. 755-757.
92. Bengtsson, A., Henriksson, K.G., and Larsson, J., *Muscle Biopsy in Primary Fibromyalgia - Light-Microscopic and Histochemical Findings.* Scandinavian Journal of Rheumatology, 1986. **15**(1): p. 1-6.
93. Lund, N., Bengtsson, A., and Thorborg, P., *Muscle-Tissue Oxygen-Pressure in Primary Fibromyalgia.* Scandinavian Journal of Rheumatology, 1986. **15**(2): p. 165-173.
94. Bengtsson, A., Henriksson, K.G., and Larsson, J., *Reduced High-Energy Phosphate Levels in the Painful Muscles of Patients with Primary Fibromyalgia.* Arthritis and Rheumatism, 1986. **29**(7): p. 817-821.
95. Park, J.H., Phothimat, P., Oates, C.T., Hernanz-Schulman, M., and Olsen, N.J., *Use of P-31 magnetic resonance spectroscopy to detect metabolic abnormalities in muscles of patients with fibromyalgia.* Arthritis and Rheumatism, 1998. **41**(3): p. 406-413.
96. Mook, P.H., Proctor, H.J., Jobsis, F., and Wildevuur, C.R., *Assessment of brain oxygenation: a comparison between an oxygen electrode and near-infrared spectrophotometry.* Advances in Experimental Medicine and Biology, 1984. **169**: p. 841-847.
97. Colacino, J.M., Grubb, B., and Jobsis, F.F., *Infra-red technique for cerebral blood flow: comparison with 133Xenon clearance.* Neurological Research, 1981. **3**(1): p. 17-31.
98. Roberts, I., Fallon, P., Kirkham, F.J., Lloydthomas, A., Cooper, C., Maynard, R., Elliot, M., and Edwards, A.D., *Estimation of Cerebral Blood-Flow with near-Infrared Spectroscopy and Indocyanine Green.* Lancet, 1993. **342**(8884): p. 1425-1425.
99. Hongo, K., Kobayashi, S., Okudera, H., Hokama, M., and Nakagawa, F., *Noninvasive Cerebral Optical Spectroscopy - Depth-Resolved Measurements of Cerebral Hemodynamics Using Indocyanine Green.* Neurological Research, 1995. **17**(2): p. 89-93.
100. Patel, J., Marks, K., Roberts, I., Azzopardi, D., and Edwards, A.D., *Measurement of cerebral blood flow in newborn infants using near infrared spectroscopy with indocyanine green.* Pediatric Research, 1998. **43**(1): p. 34-39.
101. Kindig, C.A., Richardson, T.E., and Poole, D.C., *Skeletal muscle capillary hemodynamics from rest to contractions: implications for oxygen transfer.* Journal of Applied Physiology, 2002. **92**(6): p. 2513-2520.

102. Tschakovsky, M.E. and Hughson, R.L., *Ischemic muscle chemoreflex response elevates blood flow in nonischemic exercising human forearm muscle.* American Journal of Physiology, 1999. **277**(2 Pt 2): p. H635-H642.
103. Mayrovitz, H.N. and Delgado, M., *Effect of compression bandaging on lower extremity skin microcirculation.* Wounds-a Compendium of Clinical Research and Practice, 1996. **8**(6): p. 200-207.
104. Bochmann, R.P., Seibel, W., Haase, E., Hietschold, V., Rodel, H., and Deussen, A., *External compression increases forearm perfusion.* Journal of Applied Physiology, 2005. **99**(6): p. 2337-2344.
105. Van Beekvelt, M.C., van Engelen, B.G.M., Wevers, R.A., and Colier, W.N.J.M., *Quantitative near-infrared spectroscopy discriminates between mitochondrial myopathies and normal muscle.* Annals of Neurology, 1999. **46**(4): p. 667-670.
106. Hoppeler, H., Hudlicka, O., and Uhlmann, E., *Relationship between Mitochondria and Oxygen-Consumption in Isolated Cat Muscles.* Journal of Physiology-London, 1987. **385**: p. 661-675.
107. Homma, S., Eda, H., Ogasawara, S., and Kagaya, A., *Near-infrared estimation of O-2 supply and consumption in forearm muscles working at varying intensity.* Journal of Applied Physiology, 1996. **80**(4): p. 1279-1284.
108. Merton, P.A., *Voluntary Strength and Fatigue.* Journal of Physiology-London, 1954. **123**(3): p. 553-564.
109. Bennett, R.M., Clark, S.R., Goldberg, L., Nelson, D., Bonafede, R.P., Porter, J., and Specht, D., *Aerobic fitness in patients with fibrositis. A controlled study of respiratory gas exchange and 133xenon clearance from exercising muscle.* Arthritis and Rheumatism, 1989. **32**(4): p. 454-460.
110. Olive, J.L., DeVan, A.E., and McCully, K.K., *The effects of aging and activity on muscle blood flow.* Dyn Med, 2002. **1**(2).
111. DeLorey, D.S., Kowalchuk, J.M., and Paterson, D.H., *Effect of age on O-2 uptake kinetics and the adaptation of muscle deoxygenation at the onset of moderate-intensity cycling exercise.* Journal of Applied Physiology, 2004. **97**(1): p. 165-172.
112. Wang, Z.Y., Noyszewski, E.A., and Leigh, J.S., *Invivo Mrs Measurement of Deoxymyoglobin in Human Forearms.* Magnetic Resonance in Medicine, 1990. **14**(3): p. 562-567.
113. Mancini, D.M., Bolinger, L., Li, H., Kendrick, K., Chance, B., and Wilson, J.R., *Validation of near-Infrared Spectroscopy in Humans.* Journal of Applied Physiology, 1994. **77**(6): p. 2740-2747.
114. Schenkman, K.A., Marble, D.R., Burns, D.H., and Feigl, E.O., *Myoglobin oxygen dissociation by multiwavelength spectroscopy.* Journal of Applied Physiology, 1997. **82**(1): p. 86-92.
115. Hampson, N.B. and Piantadosi, C.A., *Near-Infrared Monitoring of Human Skeletal-Muscle Oxygenation during Forearm Ischemia.* Journal of Applied Physiology, 1988. **64**(6): p. 2449-2457.
116. Ripoll, J., Ntziachristos, V., Culver, J.P., Pattanayak, D.N., Yodh, A.G., and Nieto-Vesperinas, M., *Recovery of optical parameters in multiple-layered diffusive media: theory and experiments.* Journal of the Optical Society of America a-Optics Image Science and Vision, 2001. **18**(4): p. 821-830.

117. Niwayama, M., Lin, L., Shao, J., Kudo, N., and Yamamoto, K., *Quantitative measurement of muscle hemoglobin oxygenation using near-infrared spectroscopy with correction for the influence of a subcutaneous fat layer.* Review of Scientific Instruments, 2000. **71**(12): p. 4571-4575.
118. Dawson, D., Vincent, M.A., Barrett, E.J., Kaul, S., Clark, A., Leong-Poi, H., and Lindner, J.R., *Vascular recruitment in skeletal muscle during exercise and hyperinsulinemia assessed by contrast ultrasound.* American Journal of Physiology-Endocrinology and Metabolism, 2002. **282**(3): p. E714-E720.
119. Lai, N., Zhou, H.Y., Saidel, G.M., Wolf, M., McCully, K., Gladden, L.B., and Cabrera, M.E., *Modeling oxygenation in venous blood and skeletal muscle in response to exercise using near-infrared spectroscopy.* Journal of Applied Physiology, 2009. **106**(6): p. 1858-1874.
120. Kagaya, A. and Ogita, F., *Blood flow during muscle contraction and relaxation in rhythmic exercise at different intensities.* Annals of Physiological Anthropology, 1992. **11**(3): p. 251-256.
121. Saltin, B., Radegran, G., Koskolou, M.D., and Roach, R.C., *Skeletal muscle blood flow in humans and its regulation during exercise.* Acta Physiologica Scandinavica, 1998. **162**(3): p. 421-436.
122. Gurley, K., Shang, Y., and Yu, G., *Noninvasive optical quantification of absolute blood flow, blood oxygenation, and oxygen consumption rate in exercising skeletal muscle.* Journal of Biomedical Optics, 2012. **17**(7): p. 075010.

VITA

KATELYN GURLEY

Current Positions

8/2010 – Present	Research Assistant, Bio-photonics Laboratory, Biomedical Engineering, University of Kentucky, Lexington, Kentucky

Previous Positions

5/2010 – 8/2010	Graduate Assistant/Research Mentor, NSF REU in Electrical and Computer Engineering, University of Kentucky, Lexington, Kentucky
1/2010 – 8/2010	NSF Undergraduate Research Scholar, Bone Mechanotransduction Laboratory, Biomedical Engineering, University of Kentucky, Lexington, Kentucky

Education

2005 – 2010	B.S. Electrical Engineering (Minor in Mathematics), University of Kentucky; Lexington, Kentucky

Fellowships

2010 – 2011	Jack and Linda Gill Science and Engineering Fellowship, University of Kentucky; Lexington, Kentucky
2011 – 2012	USEC Graduate Fellowship, University of Kentucky; Lexington, Kentucky

Honors

2011 – 2012	President, Biomedical Engineering Society, University of Kentucky
2010	NSF Undergraduate Research Scholar (EPSCoR)
2009 – 2010	President, Eta Kappa Nu, Electrical and Computer Engineering Honorary Society, University of Kentucky
2008	Member, Tau Beta Pi, Engineering Honorary Society, University of Kentucky
2008 & 2009	Margaret and George Peters Scholarship in Engineering, University of Kentucky
2005 – 2009	University of Kentucky Presidential Scholarship
2005	Lexington Rotary Club Fayette County Academic Scholarship, Lexington, Kentucky

Professional Memberships

2012 –	*Member*, American College of Sports Medicine
2011 –	*Member*, Optical Society of America
2010 –	*Member*, Biomedical Engineering Society
2007 –	*Member,* Institute of Electrical and Electronics Engineers (IEEE)

2005 – *Member*, Society of Women Engineers

Publications (Peer Reviewed)

1. **K. Gurley**, Y. Shang, G. Yu, *"Noninvasive optical quantification of absolute blood flow, blood oxygenation, and oxygen consumption rate in exercising skeletal muscle."* Journal of Biomedical Optics, 2012. **17**(7): p. 075010.
2. Y. Shang, **K. Gurley**, B. Symons, D. Long, R. Srikuea, L. J. Crofford, C. A. Peterson, G. Yu, *"Noninvasive optical characterization of muscle blood flow, oxygenation, and metabolism in women with fibromyalgia."* Arthritis Research and Therapy, 2012 (under revision).

Conference Abstracts

1. **K. Gurley**, Y. Shang, G. Yu, "Noninvasive optical quantification of absolute blood flow and oxygen consumption rate in exercising skeletal muscle", 59th Annual Meeting of American College of Sports Medicine (ACSM), San Francisco, CA, 2012
2. G. Yu**, K. Gurley**, Y. Shang, "DCS Measurement Can Be Gated Via Monitoring Muscle Movement to Derive Accurate Blood Flow in Exercising Muscle", OSA Biomedical Optics (BIOMED), Miami, FL, 2012
3. **K. Gurley**, Y. Shang, G. Yu, "Noninvasive Optical Quantification of Absolute Blood Flow and Oxygen Consumption Rate in Exercising Skeletal Muscle", OSA Biomedical Optics (BIOMED), Miami, FL, 2012
4. Y. Shang, **K. Gurley**, B. Symons, D. Long, J. Lee, R. Srikuea, L. Crofford, C. Peterson, G. Yu, "Diffuse optical detecting hemodynamic responses during fatiguing exercise in women with fibromyalgia", OSA Biomedical Optics (BIOMED), Miami, FL, 2012
5. Y. Shang, **K. Gurley**, B. Symons, D. Long, J. Lee, L. Crofford, C. Peterson, G. Yu, "Diffuse optical spectroscopies for detecting hemodynamic recovery in women with fibromyalgia", Gill Heart Cardiovascular Research Day, Poster Section, University of Kentucky, Lexington, KY, 2011
6. Y. Shang, **K. Gurley**, B. Symons, D. Long, J. Lee, L. Crofford, C. Peterson, G. Yu, "Diffuse optical spectroscopies for detecting hemodynamic recovery in women with fibromyalgia", UK Muscle Biology Fall Retreat, Lexington, KY, 2011
7. Y. Shang, R. Cheng, L. Dong, D. Irwin, **K. M. Gurley**, K. R. Swartz, S. S. Salles, G. Yu, "Evaluation of Electronic Stimulation Impact on Muscle hemodynamics Using Diffuse Optical Spectroscopies", 23rd Annual Physical Medicine and Rehabilitation Research Day, Lexington, KY, 2011
8. **K. Gurley**, A. Gobin, MM. Saunders, "*MicroCT assessment of bone organ culture viability and development in a neonatal rat femur model*", 15th Annual KY EPSCoR Conference, Lexington, KY, 2010.
9. DE Brittle, **KM Gurley**, AS Gobin, MM. Saunders, *"MicroCT analysis of whole bone culture viability out to one month."* Engineering Platforms for Exploring Cellular and Molecular Signaling Processes Annual Conference. University of Louisville, Louisville, KY, 2010.

10. **K. Gurley**, AS Gobin, MM. Saunders, *"A microCT assessment of bone organ culture viability in a neonatal rat femur model."* Engineering Platforms for Exploring Cellular and Molecular Signaling Processes Annual Conference. University of Louisville, Louisville, KY, 2010.
11. MM. Saunders, J. Van Sickels, B. Heil, **KM Gurley**, *"Distraction osteogenesis in organ culture."* Annals of Biomedical Engineering, Biomedical Engineering Society 2010 Annual Fall Meeting, Austin, TX, 2010.
12. **K. Gurley**, A. Gobin, MM. Saunders, *"MicroCT assessment of neonatal rat femur organ culture development."* Annals of Biomedical Engineering, Biomedical Engineering Society 2010 Annual Fall Meeting, Austin, TX, 2010.